

A dCDD-Based Transmit Diversity Scheme for Downlink Pseudo-NOMA Systems

Kim, Kyeong Jin; Liu, Hongwu; Lei, Hongjiang; Ding, Zhiguo; Orlik, Philip V.; Poor, H. Vincent

TR2020-176 January 23, 2021

Abstract

In this paper, a new transmit diversity scheme is proposed for cooperative pseudo-non-orthogonal multiple access (Pseudo-NOMA) without assuming full channel state information at the transmitter (CSIT). To support two users under the nearfar user pairing constraint, a distributed cyclic delay diversity (dCDD) scheme is adapted into NOMA by dividing a set of remote radio heads (RRHs) into two groups for multiple cyclicprefixed single carrier transmissions. To maximize a far user's rate and two users' sum rate over independently but nonidentically distributed frequency selective fading channels and under near-far user pairing constraint, we first derive the closedform expressions for the rate of two users with full CSIT. Considering that only partial CSIT is available, a new RRH assignment and power allocation scheme is proposed for dCDDPseudo-NOMA. For various simulation scenarios, the provided link-level simulations verify that the superior rate can be achieved by dCDD-Pseudo-NOMA over the traditional orthogonal multiple access with dCDD and dCDD-Conventional-NOMA that uses the superimposed signals. Furthermore, the proposed RRH assignment and power allocation scheme makes dCDD-PseudoNOMA achieves almost the same rate as that of ideal dCDDPseudo-NOMA which requires full CSIT.

IEEE Transactions on Wireless Communications

© 2021 IEEE. Personal use of this material is permitted. Permission from IEEE must be obtained for all other uses, in any current or future media, including reprinting/republishing this material for advertising or promotional purposes, creating new collective works, for resale or redistribution to servers or lists, or reuse of any copyrighted component of this work in other works.

Mitsubishi Electric Research Laboratories, Inc.
201 Broadway, Cambridge, Massachusetts 02139

A dCDD-Based Transmit Diversity Scheme for Downlink Pseudo-NOMA Systems

Kyeong Jin Kim, *Senior Member, IEEE*, Hongwu Liu, *Senior Member, IEEE*,
Hongjiang Lei, *Senior Member, IEEE*, Zhiguo Ding, *Fellow, IEEE*,
Philip V. Orlik, *Senior Member, IEEE*, and
H. Vincent Poor, *Life Fellow, IEEE*

Abstract—In this paper, a new transmit diversity scheme is proposed for cooperative pseudo-non-orthogonal multiple access (Pseudo-NOMA) without assuming full channel state information at the transmitter (CSIT). To support two users under the near-far user pairing constraint, a distributed cyclic delay diversity (dCDD) scheme is adapted into NOMA by dividing a set of remote radio heads (RRHs) into two groups for multiple cyclic-prefixed single carrier transmissions. To maximize a far user's rate and two users' sum rate over independently but non-identically distributed frequency selective fading channels and under near-far user pairing constraint, we first derive the closed-form expressions for the rate of two users with full CSIT. Considering that only partial CSIT is available, a new RRH assignment and power allocation scheme is proposed for dCDD-Pseudo-NOMA. For various simulation scenarios, the provided link-level simulations verify that the superior rate can be achieved by dCDD-Pseudo-NOMA over the traditional orthogonal multiple access with dCDD and dCDD-Conventional-NOMA that uses the superimposed signals. Furthermore, the proposed RRH assignment and power allocation scheme makes dCDD-Pseudo-NOMA achieves almost the same rate as that of ideal dCDD-Pseudo-NOMA which requires full CSIT.

Index Terms—Distributed cyclic delay diversity, Pseudo-NOMA, cyclic-prefixed single carrier transmissions, near-far user pairing, RRH cooperation, QRD-M, power allocation, rate.

I. INTRODUCTION

BECAUSE of its capability to meet high spectral efficiency, ultra-reliability, and low-latency required by tactile Internet, mobile edge computing, and beyond fifth generation (B5G) networks, non-orthogonal multiple access (NOMA) has emerged as a key technique for the upcoming decade of wireless communication evolutions [2]–[4]. With

This article was presented in part at the 2020 IEEE International Conference on Communications [1]. (*corresponding author: Kyeong Jin Kim*)

Kyeong Jin Kim and Philip V. Orlik are with Mitsubishi Electric Research Laboratories (MERL), Cambridge, MA 02139 USA (e-mail: kkim@merl.com; porlik@merl.com).

Hongwu Liu is with the School of Information Science and Electrical Engineering, Shandong Jiaotong University, Jinan 250357, China (e-mail: hong.w.liu@hotmail.com).

Hongjiang Lei is with the Chongqing Key Laboratory of Mobile Communications Technology, Chongqing University of Posts and Telecommunications, Chongqing 400065, China, and also with the Shaanxi Key Laboratory of Information Communication Network and Security, Xian University of Posts and Telecommunications, Xian 710121, China (e-mail: leihj@cqupt.edu.cn).

Zhiguo Ding is with the School of Electrical and Electronic Engineering, The University of Manchester, Manchester M13 9PL, U.K. (e-mail: zhiguo.ding@manchester.ac.uk).

H. Vincent Poor is with the Department of Electrical Engineering, Princeton University, Princeton, NJ 08544 USA (e-mail: poor@princeton.edu).

the aid of superposition coding in the power-domain, multiple users are multiplexed on the same time-frequency resource block with different power levels. To mitigate intra-cluster interference inherited from the NOMA principle, successive interference cancellation (SIC) is in general applied at the receiver side to recover the signal [5].

To enhance system performance and provide new degrees of freedom (DoF), various diversity techniques were applied in NOMA systems, including multiple-input multiple-output (MIMO) antennas techniques and cooperative transmission schemes. Compared to conventional MIMO orthogonal multiple access (OMA), MIMO-NOMA can achieve a larger diversity order meanwhile serving more users [6]. It has been shown in [6] and [7] that channel gain disparity affects the diversity order achieved by NOMA users. To achieve the full diversity for NOMA systems, signal alignment and transmit power allocation were proposed by [8] and [9]. In [10], user grouping and transmit power allocation were jointly optimized to improve the system performance achieved by downlink beamforming. To avoid sophisticated channel ordering required by SIC, MIMO-NOMA can be decomposed into single-input single-output (SISO) NOMA with a greatly decreased complexity [5]. However, power allocation and user ordering in MIMO-NOMA systems make the system performance evaluation more challenging over that of SISO-NOMA systems [11].

To support a cell-edge user for downlink NOMA systems, coordinated two-transmitter employing Alamouti code was proposed in [12]. By sorting the users in their quality-of-service (QoS) requirements, the impact of relay selection schemes on performance of cooperative NOMA was investigated in [13] and [14] and two-stage relay selection protocols were proposed for cooperative NOMA systems with fixed power allocation and adaptive power allocation, respectively. These existing results show that the diversity gain for the two-stage decode-and-forward (DF) relaying scheme is proportional to the number of relays. Similar results were obtained in [15], where the users were ordered by channel conditions.

With the capability of reducing peak-to-average power ratio (PAPR) and providing robust to carrier frequency offset, cyclic-prefixed single carrier (CP-SC) transmissions were applied for distributed cyclic delay diversity (dCDD) systems to achieve the transmit diversity and frequency-selective diversity without requiring full channel state information at the transmitter (CSIT). Owing to this benefit, several types of CP-

SC transmission have applied dCDD in different distributed systems, for example, cooperative communication systems [16]–[18]; underlaying spectrum sharing systems [19], [20]; and physical layer secrecy (PLS) systems [21], [22]. However, these existing works assume only one information data stream. Considering frequency-selective fading channels, CP-SC was also applied in uplink NOMA systems, where rate splitting was proposed to decrease the outage probability for the paired users [23], [24]. Motivated by this, we apply dCDD as a new transmit diversity approach for a downlink Pseudo-NOMA system.

In contrast to existing work, our main contributions can be summarized as follows.

- To achieve the transmit diversity gain without requiring full CSIT, the dCDD scheme is employed among spatially distributed central unit (CU), remote radio heads (RRHs), and two users. Furthermore, to support near-far user pairing for NOMA [25], we adopt the original dCDD scheme as follows:
 - The CU divides a set of available RRHs into two groups based on partial CSIT that specifies the channel strength. Thus, both users need to feed back only limited information for this purpose. Each group transmits its own information signal to two users simultaneously. The proposed transmission scheme is different from the existing NOMA scheme that transmits the superimposed signals, which is called the conventional-NOMA (C-NOMA), so that the proposed NOMA is called the Pseudo-NOMA.
 - For two separate groups, the CU allocates a different power to meet the near-far user pairing constraint.
- Due to different locations of two users, non-identical frequency selective fading channels from the RRHs to two users are considered. Over realistic and challenging channels, we provide an analytical framework jointly taking into account a different degree of RRH cooperation via the dCDD protocol and power allocation.

A. Organization

The rest of the paper is organized as follows. In Section II, we detail the system and channel model of the dCDD-based CP-SC Pseudo-NOMA system. After defining random quantities and deriving their distributions, performance analysis of the dCDD-based CP-SC Pseudo-NOMA system is conducted in Section III. Simulation results are presented in Section IV, conclusions and future works are drawn in Section V.

B. Notation

\mathbb{C} denotes the set of complex numbers; \mathbb{R} denotes the set of real numbers; I_Q denotes the Q -by- Q identity matrix; and $\mathbf{0}_{m \times n}$ denotes the m -by- n zero matrix. $\mathcal{CN}(\mu, \sigma^2)$ denotes the circularly symmetric complex Gaussian distribution with mean μ and variance σ^2 ; $F_\varphi(\cdot)$ and $f_\varphi(\cdot)$ respectively denote the cumulative distribution function (CDF) and probability density function (PDF) of the random variable (RV) φ ; and $E\{\cdot\}$ denotes expectation. $\binom{n}{k} \triangleq \frac{n!}{(n-k)!k!}$ denotes

the binomial coefficient. Cardinalities of a vector \mathbf{a} and a list \mathbb{S} are respectively denoted by $|\mathbf{a}|$ and $|\mathbb{S}|$. In addition, $\sum_{\{l_1, \dots, l_L\} \setminus \{l_a, l_b\}}^{\{M_1, \dots, M_L\} \setminus \{M_a, M_b\}} \triangleq \sum_{l_1=0}^{M_1} \dots \sum_{l_{a-1}=0}^{M_{a-1}} \sum_{l_{a+1}=0}^{M_{a+1}} \dots \sum_{l_{L-1}=0}^{M_{L-1}} \sum_{l_{L+1}=0}^{M_{L+1}}$; $\sum_{l_{b-1}=0}^{M_{b-1}} \sum_{l_{b+1}=0}^{M_{b+1}} \dots \sum_{l_L=0}^{M_L} ; \sum_{\substack{n_1, \dots, n_J \\ n_1 \neq n_2 \neq \dots \neq n_J}}^B \triangleq \sum_{n_1=1}^B \dots \sum_{\substack{n_2=1 \\ n_2 \neq n_1}}^B \dots \sum_{\substack{n_J=1 \\ n_J \neq n_1, \dots, n_J \neq n_{J-1}}}^B$; and $\sum_{k_1, \dots, k_J=b}^B$ denotes the sum for all k_i s satisfying $\sum_{i=1}^J k_i = b$, each of k_i s is an integer with a maximum of b . In specifying a channel related quantity, f_i denotes the i th vector channel with its corresponding channel matrix denoted by \mathbf{F}_i , and with $N_{f,i}$ denoting the number of multipath components of f_i , i.e., $N_{f,i} = |\mathbf{f}_i|$. In addition, subscripts are used to identify an element from a particular set. For a set of continuous RVs, $\{x_1, x_2, \dots, x_N\}$, $x_{\langle i \rangle}$ denotes the i th smallest RV. For the order statistics, $\{x_{\langle 1 \rangle}, \dots, x_{\langle N \rangle}\}$, the spacing statistics, $\{y_1, \dots, y_N\}$, are defined by $y_1 = x_{\langle 1 \rangle}$ and $y_n = x_{\langle n \rangle} - x_{\langle n-1 \rangle}$ for $2 \leq n \leq N$, so that $x_{\langle n \rangle} = \sum_{i=1}^n y_i$. The Jacobian matrix for the change of variables is lower triangular with ones on its diagonal, so that its determinant is one.

II. SYSTEM AND CHANNEL MODEL

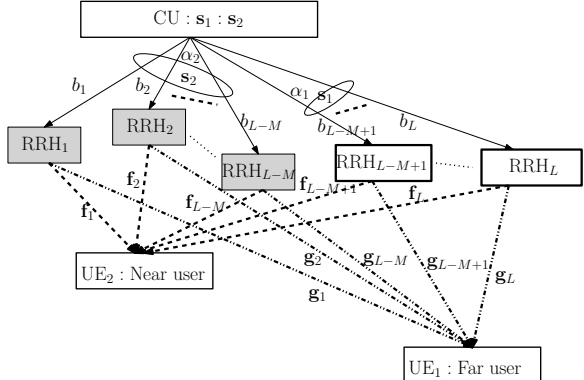


Fig. 1. Illustration of the proposed dCDD-based cooperative Pseudo-NOMA system with L RRHs and two users, UE₁ and UE₂.

Fig. 1 illustrates a block diagram of the cooperative Pseudo-NOMA system considered in this paper, which comprises a single CU, L RRHs, and two users¹, i.e., UE₁ and UE₂. The set of RRHs, $\{\text{RRH}_i\}_{i=L-M+1}^L$, appears as the first group. Similarly another set of RRHs, $\{\text{RRH}_i\}_{i=1}^{L-M}$, appears as the second group. Only one antenna is assumed to be deployed at each of the two users and RRHs due to hardware and power constraints. It is assumed that UE₁ is far away than UE₂ from RRHs, so that UE₁ appears as a far user in the considered system. For this cooperative and distributed system, the CU specifies how to control L RRHs [16] via dedicated highly reliable backhauls², $\{b_l\}_{l=1}^L$. The CU forms two independent

¹Although this paper assumes only two users, more users can be considered as an extension. However, a tight restriction on power allocation and RRH assignment is required due to an employed near-far user pairing constraint.

²In contrast to the works [26]–[28], we assume optical fiber backhaul [29], such that a limited backhaul capacity and unreliable backhaul is beyond of the scope of this paper. With an installation of a single antenna at the RRHs, the set of RRHs can be configured as a distributed antenna system and coordinated multiple point (CoMP) with additional hardware resources [20], [29]–[33].

information signals, s_1 and s_2 being transmitted simultaneously to UE₁ and UE₂. The half-duplex constraint is assumed for all the users and RRHs.

As a transmit diversity scheme, dCDD is employed [16]. It has been known that the maximum number of RRHs for dCDD operation is limited by the transmission symbol block size³ and the maximum number of multipath components over frequency selective fading channels connected from L RRHs to UE₁ and UE₂. Thus, this paper investigates only a finite-sized cooperative NOMA system comprising a finite number of L RRHs for full dCDD operation and two users. By employing appropriate channel sounding schemes or channel reciprocity [34], [35], we further assume that each user is able to know the maximum number of multipath components of the channels connected to the RRHs. Note that dCDD has a very similar handshaking message overhead compared with TAS, wherein the receiver conveys the antenna index to the transmitting side for CP-SC transmissions. Since the considered system employs inter-symbol interference (ISI)-free CP-SC transmissions, each user needs to feed back the maximum number of multipath components of the channels connected to L RRHs.

The following channels are assumed in the proposed system.

- Channels from L RRHs to UE₁: A multipath channel from the m th RRH to UE₁ is given by $\mathbf{g}_m = \sqrt{(d_{1,m})^{-\epsilon_L}} \tilde{\mathbf{g}}_m$, where $\tilde{\mathbf{g}}_m$ denotes the m th frequency selective fading channel with $N_{g,m} \triangleq |\tilde{\mathbf{g}}_m|$ multipath components. A distance from the m th RRH to UE₁ is given by $d_{1,m}$. The path loss exponent over channel \mathbf{g}_m is denoted by ϵ_L . In addition, we assume that $d_{1,m} \neq d_{1,n}, \forall m, n$.
- Channels from L RRHs to UE₂: A multipath channel, \mathbf{f}_m , from the m th RRH to UE₂ is given by $\mathbf{f}_m = \sqrt{(d_{2,m})^{-\epsilon_L}} \tilde{\mathbf{f}}_m$, where $\tilde{\mathbf{f}}_m$ specifies the m th frequency selective fading channel with $N_{f,m} \triangleq |\tilde{\mathbf{f}}_m|$ multipath components. A distance from the m th RRH to UE₂ is given by $d_{2,m}$. It is also assumed that $d_{2,m} \neq d_{2,n}, \forall m, n$. Since \mathbf{f}_m is connected only by RRH _{m} , and UE₂ is widely separated from UE₁, the channel gains, $\{\mathbf{g}_m\}_{m=1}^L$ and $\{\mathbf{f}_m\}_{m=1}^L$, are assumed to be uncorrelated.
- The multipath components of all frequency selective fading channels are assumed to be independent and identically distributed (i.i.d.) according to $\mathcal{CN}(0, 1)$. However, due to different distances from L RRHs to UE₁ and UE₂, a composite frequency selective fading channel comprising small and large-scale fading is distributed independently but non-identically distributed (i.n.i.d.) in the whole system. We also assume that all the channels are constant over one symbol block transmission interval due to the quasi-static channel assumption, but independent from those for other transmission intervals.

A. dCDD for CP-SC Transmissions

To make dCDD properly working in the Pseudo-NOMA system, we briefly summarize dCDD as follows [16].

³Since CP-SC transmission is used in the considered system, transmission symbols s_1 and s_2 are composed of B modulated symbols.

- 1) Since the original dCDD allows L RRHs to transmit the same block symbols s at the same time, it is necessary to remove possible ISI at the receiver. In addition, due to transmissions in the multipath fading channel, ISI will be observed at the receiver. Thus, multiple transmissions and frequency selective fading cause ISI at the receiver. Channel-related ISI can be removed by appending the last N_{CP} symbols of $s \in \mathbb{C}^{B \times 1}$ to the front of s , where N_{CP} denotes the CP length [36]. From the employed channel model, $N_{g,CP}$ and $N_{f,CP}$ are determined respectively by UE₁ and UE₂ as follows: $N_{g,CP} \triangleq \max(N_{g,m}), \forall m$ and $N_{f,CP} \triangleq \max(N_{f,m}), \forall m$. After receiving $N_{g,CP}$ and $N_{f,CP}$ by feeding back from UE₁ and UE₂, the CU determines N_{CP} as $N_{CP} \triangleq \max(N_{g,CP}, N_{f,CP})$. Based on N_{CP} , the CU assigns the CDD delay, as a function of N_{CP} , to every RRH. According to [16], the m th CDD delay is given by $\Delta_m = (m - 1)N_{CP}$. Note that when $\Delta_m \neq \Delta_n, \forall m, n$ with $m \neq n$, a particular CDD delay assignment does not cause any performance differences when the maximum-likelihood detector is used at the receiver [16], [36], [37]. For example, when Δ_m is assigned to the RRH sequentially, it is called a linear mapping.
- 2) The block size of the information symbol, denoted by B , is determined by CP-SC transmissions [36], that is, B is known at the CU. To achieve ISI-free reception at the receiver from multiple CP-SC transmissions, the CU needs to determine the maximum allowable number of RRHs for dCDD as follows: $K = \lfloor B/N_{CP} \rfloor$, where $\lfloor \cdot \rfloor$ denotes the floor function. In general, N_{CP} is specified by $N_{CP} = B/4$ in wireless systems [38], [39], so that four RRHs can be available for dCDD. When the system is overpopulated, K RRHs that are resulting in greater channel strength at UE₁ are selected in order to reduce system overhead caused by the coordination of the RRHs. The remaining RRHs are not allowed by the CU to transmit signals. To simplify the performance analysis, we assume an underpopulated system that comprises L RRHs, with $L \leq K$. Since the proposed system is required to transmit two independent symbol blocks, $s_1 \in \mathbb{C}^{B \times 1}$ and $s_2 \in \mathbb{C}^{B \times 1}$, it is necessary to adjust the original dCDD scheme.
- 3) The channel strength of \mathbf{g}_m measured at UE₁ is given by $\lambda_m \triangleq \|\mathbf{g}_m\|^2$. For available L channel strengths, UE₁ arranges them as $0 < \lambda_{\langle 1 \rangle} \leq \dots \leq \lambda_{\langle L \rangle} < \infty$ and the corresponding list specifying a set of channel strengths arranged in an ascending order is defined by $\mathbb{X}_g \triangleq [\langle 1 \rangle, \dots, \langle L \rangle]$. When more than K RRHs are available in the system, UE₁ selects only K RRHs based on the channel strength, and then forms the list, $\mathbb{X}_g \triangleq [\langle 1 \rangle, \dots, \langle K \rangle]$. After receiving this list, the CU prevents $L - K$ RRHs, which are not determined by \mathbb{X}_g , from transmission. Thus, interference from $L - K$ RRHs can be removed during dCDD operation.
- 4) From 1) to 3), UE₁ needs to feed back $N_{g,CP}$ and \mathbb{X}_g to the CU, whereas UE₂ needs to feed back only $N_{f,CP}$

to the CU. Thus, the employed dCDD requires only a partial CSIT for its operation.

B. dCDD for CP-SC-Pseudo-NOMA Transmissions

Considering that U_1 and U_2 are the far and near users, respectively, more transmit power should be allocated to the U_1 's signal according to the NOMA principle. To meet these heterogeneous constraints and considering only L available RRHs for cooperative CP-SC transmissions, this paper modifies the original dCDD [16] as follows:

- RRHs are grouped to generate a relatively higher received power for s_1 and a relatively lower received power for s_2 . Based on the available \mathbb{X}_g , the CU divides L RRHs into two groups⁴ for multiple transmissions as follows:
 - First group: This group is composed by M RRHs, each of which is indexed by the set $\mathbb{S}_1 \stackrel{\Delta}{=} [\langle L-M+1 \rangle, \dots, \langle L \rangle] \subset \mathbb{X}_g$, and transmits s_1 .
 - Second group: This group is composed by the remaining $(L-M)$ RRHs, each of which is indexed by the set $\mathbb{S}_2 \stackrel{\Delta}{=} [\langle 1 \rangle, \dots, \langle L-M \rangle] \stackrel{\Delta}{=} \mathbb{X}_g - \mathbb{S}_1$, and transmits s_2 . Since \mathbb{S}_2 is mainly determined by the channels connected to UE_1 , it should be shared with UE_2 by interaction with the CU.
- After having applied a group separation for L RRHs, the CU assigns the CDD delays to every RRH. Furthermore, the CU allocates a greater power to the RRHs included in \mathbb{S}_1 .

Based on this unique feature of dCDD, we can describe the signal received at UE_1 and UE_2 as follows.

a) *Received signal at UE_1 :* Having applied dCDD, the received signal at UE_1 is given by

$$\mathbf{r}_1 = \sqrt{\alpha_1 P_s} \sum_{m=L-M+1}^L (d_{1,\langle m \rangle})^{-\epsilon_L/2} \tilde{\mathbf{G}}_{\langle m \rangle} \tilde{\mathbf{s}}_{1,m} + \left[\sqrt{\alpha_2 P_s} \sum_{m=1}^{L-M} (d_{1,\langle m \rangle})^{-\epsilon_L/2} \tilde{\mathbf{G}}_{\langle m \rangle} \tilde{\mathbf{s}}_{2,m} \right]_{J_1} + \mathbf{z}_1 \quad (1)$$

where P_s is the peak transmission power at the all RRHs, and $\tilde{\mathbf{G}}_{\langle m \rangle}$ denotes the right circulant channel matrix determined by $\tilde{\mathbf{g}}_{\langle m \rangle}$. The additive noise over all the frequency selective fading channels is denoted by $\mathbf{z}_1 \sim \mathcal{CN}(\mathbf{0}, \sigma_z^2 \mathbf{I}_B)$. In addition, α_i , with $\alpha_2 = 1 - \alpha_1$, denotes the power allocation coefficient for UE_i in transmitting s_i . The m th transformed block symbols $\tilde{\mathbf{s}}_{1,m}$ and $\tilde{\mathbf{s}}_{2,m}$ are defined as $\tilde{\mathbf{s}}_{1,m} = \mathbf{P}_{\Delta_m} s_1$ and $\tilde{\mathbf{s}}_{2,m} = \mathbf{P}_{\Delta_{\tilde{m}}} s_2$, where $m \in \mathbb{S}_1$ and $\tilde{m} \in \mathbb{S}_2$. The permutation shifting matrices $\mathbf{P}_{\Delta_m} \in \mathbb{C}^{B \times B}$ and $\mathbf{P}_{\Delta_{\tilde{m}}} \in \mathbb{C}^{B \times B}$ can be obtained from the identity matrix \mathbf{I}_B by respectively circularly shifting down by Δ_m and $\Delta_{\tilde{m}}$. Note that $[\cdot]_{J_1}$ is the interfering signal at UE_1 . By simultaneously taking into account the power allocation and the use of set \mathbb{S}_1 for the transmissions of s_1 , UE_1 can achieve a desired rate even in the presence of interfering signals.

With the use of permutation matrices, (1) can be rewritten as follows:

$$\mathbf{r}_1 = \sqrt{\alpha_1 P_s} \sum_{m=L-M+1}^L (d_{1,\langle m \rangle})^{-\epsilon_L/2} \tilde{\mathbf{G}}_{\langle m \rangle} \mathbf{P}_{\Delta_m} s_1 +$$

⁴When three users exist in the system, the CU needs to divides \mathbb{X}_g into three groups with $|\mathbb{S}_1| = M$, $|\mathbb{S}_2| = L - M - L_1$, and $|\mathbb{S}_3| = L_1$, where \mathbb{S}_1 , \mathbb{S}_2 , and \mathbb{S}_3 respectively determine RRHs to transmit s_1 , s_2 , and s_3 .

$$\sqrt{\alpha_2 P_s} \sum_{m=1}^{L-M} (d_{1,\langle m \rangle})^{-\epsilon_L/2} \tilde{\mathbf{G}}_{\langle m \rangle} \mathbf{P}_{\Delta_{\tilde{m}}} s_2 + \mathbf{z}_1 \quad (2)$$

where $\tilde{\mathbf{G}}_{\langle m \rangle} \mathbf{P}_{\Delta_m}$ and $\tilde{\mathbf{G}}_{\langle m \rangle} \mathbf{P}_{\Delta_{\tilde{m}}}$ are right circulant matrices.

b) *Received signal at UE_2 :* Similar to (2), the received signal at UE_2 is given by

$$\begin{aligned} \mathbf{r}_2 &= \sqrt{\alpha_1 P_s} \sum_{\substack{m \in \mathbb{S}_1, \\ |\mathbb{S}_1|=M}} (d_{2,m})^{-\epsilon_L/2} \tilde{\mathbf{F}}_m \mathbf{P}_{\Delta_m} s_1 + \\ &\quad \sqrt{\alpha_2 P_s} \sum_{\substack{m \in \mathbb{S}_2, \\ |\mathbb{S}_2|=L-M}} (d_{2,m})^{-\epsilon_L/2} \tilde{\mathbf{F}}_m \mathbf{P}_{\Delta_{\tilde{m}}} s_2 + \mathbf{z}_2 \end{aligned} \quad (3)$$

where we assume that $\mathbf{z}_2 \sim \mathcal{CN}(\mathbf{0}, \sigma_z^2 \mathbf{I}_B)$. Recall that $|\mathbb{S}_1|$ and $|\mathbb{S}_2|$ respectively denote the cardinality of \mathbb{S}_1 and \mathbb{S}_2 . Since $\tilde{\mathbf{F}}_m$ is determined by $\tilde{\mathbf{f}}_m$, $\tilde{\mathbf{F}}_m \mathbf{P}_{\Delta_m}$ and $\tilde{\mathbf{F}}_m \mathbf{P}_{\Delta_{\tilde{m}}}$ are right circulant matrices. From Eqs. (2) and (3), we extract the following facts:

- The received signal at UE_2 depends on the order statistics in assigning CDD delays. However, the performance of CP-SC-NOMA does not depend on its assignment [16]. Thus, it is not necessary to use the order statistics in analyzing the performance of UE_2 . In contrast, the order statistics are related with large-scale and small-scale fadings, and CDD delay assignment for UE_1 , so that it is necessary to use the order statistics in analyzing the performance of UE_1 .
- The selection mechanism for \mathbb{S}_1 and \mathbb{S}_2 will be critical in achieving the balanced rate of UE_1 and UE_2 . However, the CU has only B , N_{CP} , \mathbb{X}_g , \mathbb{S}_1 , and \mathbb{S}_2 for controlling the RRHs by dCDD. Thus, the CU uses only a partial CSIT for CP-SC-NOMA.

III. PERFORMANCE ANALYSIS OF CP-SC-PSEUDO-NOMA TRANSMISSIONS WITH DCDD

A. Operation at UE_2

UE_2 starts decoding s_1 . After then, it decodes s_2 . Thus, according to (3), the receive SNR for the decoding of s_1 is given by $\gamma_{2,s_1} = \frac{\alpha_1 A}{\alpha_2 B + 1}$, where $A \stackrel{\Delta}{=} \sum_{\substack{m \in \mathbb{S}_1, \\ |\mathbb{S}_1|=M}} Pr_m \|\tilde{\mathbf{f}}_m\|^2 / \beta_{2,m}$ and $B \stackrel{\Delta}{=} \sum_{\substack{m \in \mathbb{S}_2, \\ |\mathbb{S}_2|=L-M}} Pr_m \|\tilde{\mathbf{f}}_m\|^2 / \beta_{2,m}$ with $\rho \stackrel{\Delta}{=} P_s / \sigma_z^2$ denoting the transmit SNR, $1/\beta_{2,m} \stackrel{\Delta}{=} \rho (d_{2,m})^{-\epsilon_L}$, and Pr_m denoting the selection probability of RRH $_{m=a}$ for $a \in \{\mathbb{S}_1, \mathbb{S}_2\}$. Furthermore, we have assumed that $E\{s_j\} = \mathbf{0}$ and $E\{s_j(s_j)^H\} = \mathbf{I}_B$, for $j = 1, 2$. In addition, $E\{s_i(s_j)^H\} = \mathbf{I}_B \delta_{i-j'}$ with the Kronecker delta function, $\delta_l = \begin{cases} 0 & \text{if } l \neq 0 \\ 1 & \text{if } l = 0 \end{cases}$. Note that γ_{2,s_1} can be derived empirically by the maximum-likelihood type detector for CP-SC transmissions [36], [37].

Corollary 1: The PDF of γ_{2,s_1} is given by (4). In (4), $\theta_{L,M}(\cdot, \cdot)$ and $\theta_{L,L-M}(\cdot, \cdot)$ respectively denote partial fraction (PF) coefficients, which are defined in Appendix A. The complete gamma function is denoted by $\Gamma(\cdot)$.

Proof: See Appendix A. ■

To decode s_1 by UE_2 , the whitening process is applied to (3), then the system model can be rewritten as follows:

$$\begin{aligned} \tilde{\mathbf{r}}_2 &= \mathbf{W} \sqrt{\alpha_1 P_s} \sum_{\substack{m \in \mathbb{S}_1, \\ |\mathbb{S}_1|=M}} (d_{2,m})^{-\epsilon_L/2} \tilde{\mathbf{F}}_m \mathbf{P}_{\Delta_m} s_1 + \tilde{\mathbf{z}}_2 \\ &= \mathbf{W} \mathbf{F}_{2,1} s_1 + \tilde{\mathbf{z}}_2 \end{aligned} \quad (5)$$

$$f_{\gamma_{2,s_1}}(x) = \sum_{\substack{i_1 \in \mathbb{S}_1, \\ |\mathbb{S}_1|=M}} \sum_{j_1=1}^{L_{f,i_1}} \theta_{L,M}(i_1, j_1) / \Gamma(j_1) \sum_{\substack{i_2 \in \mathbb{S}_2, \\ |\mathbb{S}_2|=L-M}} \sum_{j_2=1}^{L_{f,i_2}} \sum_{l=0}^{j_1} (\theta_{L,L-M}(i_2, j_2) / \Gamma(j_2)) (\alpha_1)^{-j_1} \binom{j_1}{l} (\alpha_2)^l \\ \Gamma(l+j_2) Pr_{i_1} Pr_{i_2} ((\alpha_2 \beta_{2,i_1} / \alpha_1) x + \beta_{2,i_2})^{-l-j_2} e^{-(\beta_{2,i_1} / \alpha_1) x} x^{j_1-1}. \quad (4)$$

where $\tilde{\mathbf{r}}_2 \triangleq \mathbf{W} \mathbf{r}_2$, $\mathbf{F}_{2,1} \triangleq \sqrt{\alpha_1 P_s} \sum_{\substack{m \in \mathbb{S}_1, \\ |\mathbb{S}_1|=M}} (d_{2,m})^{-\epsilon_L/2}$ $\tilde{\mathbf{F}}_m \mathbf{P}_{\Delta_m}$, and $\tilde{\mathbf{z}}_2 \triangleq \mathbf{W} \mathbf{z}_2 \sim \mathcal{CN}(\mathbf{0}, \mathbf{I}_Q)$. A whitening matrix \mathbf{W} is given by $\mathbf{W} = \sigma_z (\mathbf{F}_{2,2} (\mathbf{F}_{2,2})^H + \sigma_z^2 \mathbf{I}_Q)^{-1/2}$, where $\mathbf{F}_{2,2} \triangleq \sqrt{\alpha_2 P_s} \sum_{\substack{m \in \mathbb{S}_2, \\ |\mathbb{S}_2|=L-M}} (d_{2,m})^{-\epsilon_L/2} \tilde{\mathbf{F}}_m \mathbf{P}_{\Delta_m}$. To obtain a numerically stable whitening matrix, QR decomposition (QRD) is applied to a concatenated matrix, $[\mathbf{F}_{2,2}, \sigma_z \mathbf{I}_Q]^H$:

$$\begin{bmatrix} (\mathbf{F}_{2,2})^H \\ \sigma_z \mathbf{I}_Q \end{bmatrix} = \begin{bmatrix} \mathbf{Q}_{2,a} \\ \mathbf{Q}_{2,b} \end{bmatrix} \mathbf{R}_{2,2} \quad (6)$$

where $\mathbf{R}_{2,2}$ is a $Q \times Q$ upper-triangular matrix, and $\mathbf{Q}_{2,a}$ and $\mathbf{Q}_{2,b}$ are unitary matrices of dimension $Q \times Q$. Based on (6), \mathbf{W} is given by $\mathbf{W} = (\mathbf{Q}_{2,b})^H$ [40]. Then, a reliable and approximated ML decision for s_1 can be made by applying QRD-M [37] to (5), which achieves the maximum likelihood (ML) detection with a reduced computational complexity. Note that α_1 and (L, M) jointly affect the performance of QRD-M. In particular, if α_1 approaches one and most of the RRHs are assigned to transmit s_1 , the performance can be improved and decoding error propagation can be reduced. As a result, UE₂ decodes s_2 based on the following received signal

$$\hat{\mathbf{r}}_2 \triangleq \mathbf{r}_2 - \mathbf{F}_{2,1} \hat{s}_1 = \mathbf{F}_{2,2} s_2 + \mathbf{F}_{2,1} (s_1 - \hat{s}_1) + \mathbf{z}_2 \quad (7)$$

where \hat{s}_1 denotes the decision made by QRD-M.

Once again applying QRD-M to $\hat{\mathbf{r}}_2$ and $\mathbf{F}_{2,2}$, a reliable and approximated ML decision for s_2 can be made. Under the assumption that s_1 can be perfectly decoded⁵, the SNR for decoding s_2 is given by [36]

$$\gamma_{2,s_2} = \alpha_2 \sum_{\substack{m \in \mathbb{S}_2, \\ |\mathbb{S}_2|=L-M}} Pr_m \|\tilde{\mathbf{f}}_m\|^2 / \beta_{2,m}. \quad (8)$$

Applying a similar whitening matrix to (2), UE₁ can decode s_1 even in the presence of interference caused by s_2 .

Corollary 2: When L_1 RRHs, with $L_1 < L$, are included in \mathbb{S}_2 , the employed dCDD realizes the SNR, γ_{2,s_2} , whose PDF over i.n.i.d. frequency selective fading channels is given by

$$f_{\gamma_{2,s_2}}(x) = \sum_{\substack{n_1, \dots, n_{L_1} \\ n_1 \neq n_2 \neq \dots \neq n_{L_1}}}^L Pr_{n_1, \dots, n_{L_1}} \sum_{i=1}^{L_1} \sum_{j=1}^{(\mathbf{l}_f)_i} E_{m,n}(i,j) (\alpha_2)^{-j} (x)^{j-1} e^{-(\mathbf{b}_f)_i / \alpha_2 x} / \Gamma(j) \quad (9)$$

where $\mathbf{l}_f \triangleq [N_{f,n_1}, \dots, N_{f,n_{L_1}}]^T \in \mathbb{R}^{L_1}$ and $\mathbf{b}_f \triangleq [\beta_{2,n_1}, \dots, \beta_{2,n_{L_1}}]^T \in \mathbb{R}^{L_1}$ with their i th elements are denoted by $(\mathbf{l}_f)_i$ and $(\mathbf{b}_f)_i$, and $E_{m,n}(i,j)$ denotes the PF coefficients, whose steering elements are the elements of \mathbf{b}_f . The selection probability, $Pr_{n_1, \dots, n_{L_1}}$, is given by (10) provided at the top of the next page. The derivation of (10) is provided in Appendix D. Refer to unspecified definitions, such as Ψ , Φ , η_{n_i} , and r_{n_i} in Appendix B.

⁵Note that since the outage event that UE₂ cannot decode s_1 is not considered, this is a distinct feature of a typical NOMA system.

When $|\mathbb{S}_2| = 1$ and $|\mathbb{S}_2| = 2$, then PDFs of γ_{2,s_2} can be simplified, which are respectively provided in the following *Corollary 3* and *Corollary 4*.

Corollary 3: When only one RRH is included in \mathbb{S}_2 , the employed dCDD realizes the SNR, γ_{2,s_2} , whose PDF over i.n.i.d. frequency selective fading channels is given by

$$f_{\gamma_{2,s_2}}(x) = \sum_{m=1}^L Pr_m (\beta_{2,m})^{N_{f,m}} (\alpha_2)^{-N_{f,m}} (x)^{N_{f,m}-1} e^{-(\beta_{2,m} / \alpha_2) x} / \Gamma(N_{f,m}) \quad (11)$$

where

$$Pr_m = (\beta_{1,m})^{N_{g,m}} \Phi_1 \Gamma(\tilde{m}) (\tilde{\beta}_1)^{-\tilde{m}} / \Gamma(N_{g,m}) \quad (12)$$

with $\tilde{m} \triangleq \sum_{k=1, k \neq m}^L l_k + N_{g,m}$ and $\tilde{\beta}_1 \triangleq \sum_{k=1}^L \beta_{1,k}$. An additional term, Φ_1 , is defined in Appendix C.

Proof: See Appendix C for the derivation of (12). ■

Corollary 4: When two RRHs are included in \mathbb{S}_2 , i.e., $|\mathbb{S}_2| = 2$, the employed dCDD can realize the SNR, γ_{2,s_2} , whose PDF over i.n.i.d. frequency selective fading channels is given by

$$f_{\gamma_{2,s_2}}(x) = \sum_{m=1}^L \sum_{n=1, n \neq m}^L Pr_{m,n} \sum_{i=1}^2 \sum_{j=1}^{(\tilde{\mathbf{l}}_f)_i} \tilde{E}_{m,n}(i,j) (\alpha_2)^{-j} (x)^{j-1} e^{-(\tilde{\mathbf{b}}_f)_i / \alpha_2 x} / \Gamma(j) \quad (13)$$

where $\tilde{E}_{m,n}(i,j)$ denotes the PF coefficients, whose steering elements are $\beta_{2,m}$ and $\beta_{2,n}$. In addition, we have defined $\tilde{\mathbf{l}}_f \triangleq [N_{f,m}, N_{f,n}]^T \in \mathbb{R}^2$ and $\tilde{\mathbf{b}}_f \triangleq [\beta_{2,m}, \beta_{2,n}]^T \in \mathbb{R}^2$ with their i th elements are denoted by $(\tilde{\mathbf{l}}_f)_i$ and $(\tilde{\mathbf{b}}_f)_i$. The selection probability $Pr_{m,n}$ for $\mathbb{S}_2 = \{m, n\}$, where RRH_m and RRH_n respectively provide the least and second least channel strength at UE₁, can be derived as follows:

$$Pr_{m,n} = (\beta_{1,n})^{N_{g,n}} \Psi_2 \Phi_2 \Gamma(\tilde{m}) (\tilde{\beta}_{1,mn})^{-\tilde{m}} / \Gamma(N_{g,n}) \quad (14)$$

where $\tilde{m} \triangleq \sum_{k=1, k \neq \{m,n\}}^L l_k + N_{g,n} + \eta_m$, and $\tilde{\beta}_{1,mn} \triangleq \beta_{1,m} + \sum_{k=1, k \neq \{m,n\}}^L \beta_{1,k} + \beta_{1,n} r_m$. Additional terms, η_m , r_m , Ψ_2 , and Φ_2 are defined in Appendix D.

Proof: See Appendix D for the derivation of (14). ■

Note that (10), (12), and (14) are mainly determined by the channel connected from RRHs to UE₁.

B. Operation at UE₁

According to (2), the SNR in decoding s_1 is given by

$$\gamma_{1,s_1} = \frac{\alpha_1 C_{\max}^M}{\alpha_2 D_{\min}^{L-M} + 1} \quad (15)$$

where $C_{\max}^M \triangleq \sum_{m=L-M+1}^L \|\tilde{\mathbf{g}}_{\langle m \rangle}\|^2 / \beta_{1,\langle m \rangle}$, and $D_{\min}^{L-M} \triangleq \sum_{m=1}^{L-M} \|\tilde{\mathbf{g}}_{\langle m \rangle}\|^2 / \beta_{1,\langle m \rangle}$ with $1/\beta_{1,\langle m \rangle} \triangleq \rho(d_{1,\langle m \rangle})^{-\epsilon_L}$. From (15), we can observe the following facts:

$$\begin{aligned} Pr_{n_1, \dots, n_{L_1}} = & (\beta_{1,n_1})^{N_{g,n_1}} \Psi \Phi \Gamma(\sum_{i=2}^{L_1} \eta_{n_i} + \sum_{j=L_1+1}^L l_{n_j} + N_{g,n_1}) / \Gamma(N_{g,n_1}) \\ & (\sum_{i=2}^{L_1} \beta_{1,n_i} r_{n_i} + \sum_{j=L_1+1}^L \beta_{1,l_{n_j}} + \beta_{1,n_1})^{-(\sum_{i=2}^{L_1} \eta_{n_i} + \sum_{j=L_1+1}^L l_{n_j} + N_{g,n_1})}. \end{aligned} \quad (10)$$

- In contrast to the expression for γ_{2,s_1} , the order statistics are involved in the expression for γ_{1,s_1} .
- C_{\max}^M and D_{\min}^{L-M} respectively denote RVs related with the largest and smallest instantaneous SNRs, and correlated.
- Since the CU is able to recognize the sets, \mathbb{S}_1 and \mathbb{S}_2 , the selection probability is not necessary to be involved in the computation of γ_{1,s_1} .

Although the structure of (15) is popular in the performance analysis of cooperative systems, it is necessary to derive its distribution since it depends on the correlated order statistics, and the ratio of the sum of the maximum order statistics to the sum of minimum order statistics. Thus, we first derive the PDFs of C_{\max}^M and D_{\min}^{L-M} as shown in *Corollary 5*.

Corollary 5: Denote $X_k \stackrel{\triangle}{=} \|\tilde{\mathbf{g}}_{(k)}\|^2 / \beta_{1,(k)}$ the k th smallest instantaneous SNR. Using the spacing statistics [41], [42], we can first derive alternative expressions for C_{\max}^M and D_{\min}^{L-M} , which are uncorrelated each other. Then, we can compute the target PDFs for any pairs of (L, M) s as follows:

$$\begin{aligned} f_{D_{\min}^{L-M}}(t) &= \sum_{\substack{n_1, \dots, n_{L-M} \\ n_1 \neq n_2 \neq \dots \neq n_{L-M}}}^{\widetilde{L}} \sum_{i_3=1}^{L-M} \sum_{j_3=1}^{\nu_{i_3}+1} \\ &\quad E_{\min^{L-M}}(i_3, j_3) e^{-\xi_{i_3} t} t^{j_3-1} / \Gamma(j_3), \text{ and} \\ f_{C_{\max}^M}(t) &= \sum_{\substack{n_1, \dots, n_M \\ n_1 \neq n_2 \neq \dots \neq n_M}}^{\widetilde{L}} \sum_{i_4=1}^M \sum_{j_4=1}^{\mu_{i_4}+1} \\ &\quad E_{\max^M}(i_4, j_4) e^{-\zeta_{i_4} t} t^{j_4-1} / \Gamma(j_4) \end{aligned} \quad (16)$$

where unspecified terms are defined in Appendix E. Furthermore, $E_{\min^{L-M}}(\cdot, \cdot)$ and $E_{\max^M}(\cdot, \cdot)$ denoting PF coefficients are also defined in Appendix E.

Proof: See Appendix E. ■

Note that the PDFs of D_{\min}^{L-M} and C_{\max}^M are expressed as the sum of the weighted gamma distributions. Using the spacing statistics, the PDF of γ_{1,s_1} can be derived in *Corollary 6*.

Corollary 6: Based on *Corollary 5*, the PDF of γ_{1,s_1} can be derived as that of (17) provided at the top of the next page.

Proof: Refer to Appendix A for the derivation. ■

Note that *Corollary 6* provides the PDF for a general pair of (L, M) s. This is possible by the use of spacing statistics.

C. Analysis for the achievable rates

a) *Achievable rate of UE₂:* The achievable rate of UE₂ is given by

$$R_{2,(L-M)} = \int_0^\infty \log_2(1+x) f_{\gamma_{2,s_2}}(x) dx. \quad (18)$$

Having applied (8) into (18), $R_{2,(L-M)}$ is given by for $|\mathbb{S}_2| = L_1$, $|\mathbb{S}_2| = 1$, and $|\mathbb{S}_2| = 2$ are given by (19) provided at the top of the next page. The Laplace transform of a particular Meijer G-function [43, eq. (07.34.22.0003.01)], [44, eq. (2.24.3.1)] is used for the derivation of (19).

b) *Achievable rate of UE₁:* For i.n.i.d. frequency selective fading channels, the achievable rate of UE₁ is provided in the following theorem.

Theorem 1: The dCDD-based CP-SC-NOMA transmission provides UE₁ rate given by (20) provided at the top of the next page. In (20), $G_{p_1,q_1:p_2,q_2;p_3,q_3}^{m_1,0:m_2,n_2:m_3:n_3}(\cdot, \cdot : | : | : |)$ denotes the generalized bivariate Meijer G-function defined by [43, eq. (07.34.21.0081.01)] and [45].

Proof: See Appendix F. ■

IV. SIMULATIONS

The following setup is used for generating the presented simulation results.

- For CP-SC transmissions, we assume that $B = 32$ and $N_{\text{CP}} = 6$. Thus, the CU can support up to five RRHs for dCDD operation.
- Seven RRHs are placed at $\{(0, 12), (-12, 12), (-3, 12), (-9, 12), (-16.9145, 6.1564), (-6, 8), (-12, 10)\}$ in a 2-D plane. When $L \leq 5$ RRHs are selected for servicing, we choose the first L RRHs for the simulations. In contrast, when we use more than five RRHs in specific scenarios, we first select five RRHs for dCDD operation based on the received channel strength measured at UE₁.
- The two users, UE₁ and UE₂, are respectively placed at $(3, -3)$ and $(-3, 3)$.
- According to [46], we assume that $\epsilon_L = 2.09$.
- We consider a non-identical number of multipath components and a non-identical distance between two nodes in the system. Thus, a non-identical frequency selective fading is assumed for all channels in the system.
- We use a fixed $P_s = 1$ for link-level simulations.
- For performance comparisons, the dCDD based C-NOMA is also considered, where the CU prepares superimposed symbol blocks $s = \alpha_1 s_1 + \alpha_2 s_2$. Among chosen RRHs, the same dCDD operation as that of dCDD-Pseudo-NOMA is applied. The corresponding performance of the dCDD based C-NOMA is obtained by link-level simulations.

The curves obtained via link-level simulations are denoted by **Ex**, whereas analytically obtained performance curves are denoted by **An**. As an additional notation, $N_g s = \{5, 4, 3, 4\}$ means that $N_{g,1} = 5$, $N_{g,2} = 4$, $N_{g,3} = 3$, and $N_{g,4} = 4$. The same assignment is used for $N_f s$.

A. Symbol error rate

Since interference caused by coexisting multiple users is an intrinsic problem in dCDD-Pseudo-NOMA, we investigate the impact of whitening on the uncoded symbol error rate (SER). For this, we consider the scenario with $N_g s = \{4, 6, 5, 5, 4, 5, 5\}$ and $N_f s = \{4, 6, 5, 5, 4, 5, 5\}$. As the key

$$f_{\gamma_1, s_1}(x) = \sum_{n_1 \neq n_2 \neq \dots \neq n_M}^{\sim L} \sum_{i_4=1}^M \sum_{j_4=1}^{\mu_{i_4}+1} \sum_{n_1 \neq n_2 \neq \dots \neq n_{L-M}}^L \sum_{i_3=1}^{L-M} \sum_{j_3=1}^{\nu_{i_3}+1} E_{\max M}(i_4, j_4) E_{\min L-M}(i_3, j_3) \\ (\alpha_1)^{-j_4} / \Gamma(j_3) / \Gamma(j_4) \sum_{l=0}^{j_4} \binom{j_4}{l} (\alpha_2)^l \Gamma(l+j_3) e^{-(\zeta_{i_4} \alpha_1)x} x^{j_4-1} ((\alpha_2 \zeta_{i_4} / \alpha_1)x + \xi_{i_3})^{-l-j_3}. \quad (17)$$

$$R_{2,(L-M)} = \begin{cases} \frac{1}{\log(2)} \sum_{m=1}^L Pr_m(\beta_{2,m})^{N_{f,m}} (\alpha_2)^{-N_{f,m}} (\beta_{2,m}/\alpha_2)^{-N_{f,m}} / \Gamma(N_{f,m}) \\ G_{3,2}^{1,3}(\alpha_2/\beta_{2,m} | \begin{array}{c} 1-N_{f,m}, 1, 1 \\ 1, 0 \end{array}) \text{ for } (L-M)=1, \\ \frac{1}{\log(2)} \sum_{m=1}^L \sum_{n=1, n \neq m}^L Pr_{m,n} \sum_{i=1}^2 \sum_{j=1}^{(\tilde{l}_f)_i} E_{m,n}(i,j) (\alpha_2)^{-j} ((\tilde{b}_f)_i / \alpha_2)^{-j} / \Gamma(j) \\ G_{3,2}^{1,3}(\alpha_2/(\tilde{b}_f)_i | \begin{array}{c} 1-j, 1, 1 \\ 1, 0 \end{array}) \text{ for } (L-M)=2, \\ \frac{1}{\log(2)} \sum_{n_1 \neq n_2 \neq \dots \neq n_{L_1}}^L Pr_{n_1, \dots, n_{L_1}} \sum_{i=1}^{L_1} \sum_{j=1}^{(\tilde{l}_f)_i} E_{m,n}(i,j) (\alpha_2)^{-j} ((b_f)_i / \alpha_2)^{-j} / \Gamma(j) \\ G_{3,2}^{1,3}(\alpha_2/(b_f)_i | \begin{array}{c} 1-j, 1, 1 \\ 1, 0 \end{array}) \text{ for } (L-M)=L_1. \end{cases} \quad (19)$$

$$R_{1,(L,M)} = \frac{1}{\log(2)} \sum_{n_1 \neq n_2 \neq \dots \neq n_M}^{\sim L} \sum_{i_4=1}^M \sum_{j_4=1}^{\mu_{i_4}+1} \sum_{n_1 \neq n_2 \neq \dots \neq n_{L-M}}^L \sum_{i_3=1}^{L-M} \sum_{j_3=1}^{\nu_{i_3}+1} E_{\max M}(i_4, j_4) \\ E_{\min L-M}(i_3, j_3) (\alpha_1)^{-j_4} / \Gamma(j_4) / \Gamma(j_3) \sum_{l=0}^{j_4} \binom{j_4}{l} (\alpha_2)^l \Gamma(l+j_3) (\alpha_2)^{-l-j_3} (\zeta_{i_4} / \alpha_1) \\ G_{1,0;2,2;1,1}^{1,0;1,2;1,1}(\zeta_{i_4} / \alpha_1, \xi_{i_3} / \alpha_2 | \begin{array}{c} 1 \\ j_4, j_4-1 \\ j_4, j_4-1 \end{array} | \begin{array}{c} 1-l-j_3 \\ 0 \end{array}). \quad (20)$$

parameter of QRD-M [37], QRD_M that specifies the maximum number of branches at each detection stage is set to 48. For binary phase-shift keying (BPSK), Fig. 2 shows the SER for various values of (L, M) and α_1 . This figure shows the

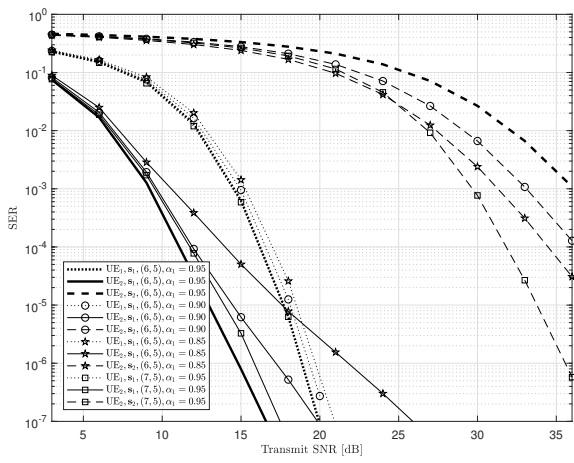


Fig. 2. SER for various system settings and α_1 s.

following observations:

- At the considered transmit SNRs, 3 – 36 dBs, a performance floor in the SER of UE₂ to decode s_2 is not

observed up to 5×10^{-7} . This benefits from the employed whitening process and the use of QRD-M.

- As α_1 increases, a lower SER can be achieved by UE₁ and UE₂ to decode s_1 . However, UE₂ results in a greater SER to decode s_2 since a less transmit power is allocated to the RRHs indexed by the set \mathbb{S}_2 .
- By employing more RRHs, UE₂ can achieve a lower SER to decode s_2 , while a greater SER is resulted from decoding s_1 by UE₁. For example, $(L=7, M=5)$ and $(L=6, M=5)$ with $\alpha_1 = 0.95$.
- Due to the employed near-far user pairing constraint, a lower SER is achieved by UE₁ and UE₂ to decode s_1 comparing with UE₂ to decode s_2 .

B. Accuracy of the derived rate

Since the derivation of the closed-form expression for $R_{1,(L,M)}$, expressed by (20), is challenging in the proposed system, we first verify its accuracy comparing with the corresponding exact rate in Fig. 3. The corresponding rate of UE₂ is provided in Fig. 4. For various combinations of (L, M) , α_1 , α_2 , and $(N_f s, N_g s)$, Figs. 3 and 4 show that (20) and (19) provide accurate analysis for the rates of UE₁ and UE₂.

C. Rate analysis

- a) *The impact of the cardinality of \mathbb{S}_1 :* We use a fixed $\alpha_1 = 0.9$ and $N_{g,m} = 2, \forall m$ to investigate the impact of the

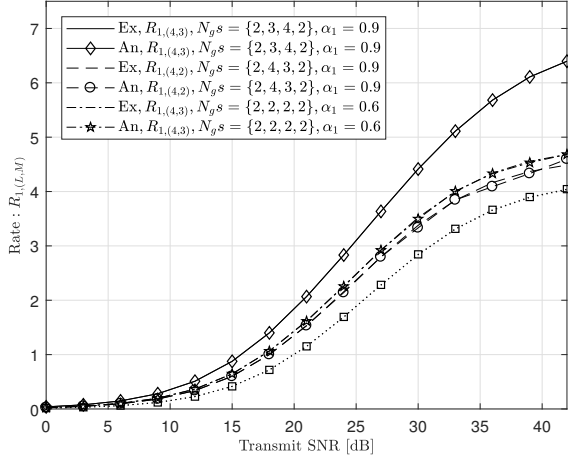


Fig. 3. Achievable rate of UE₁ for various system parameters with $N_{fs} = \{2, 2, 2, 2\}$.

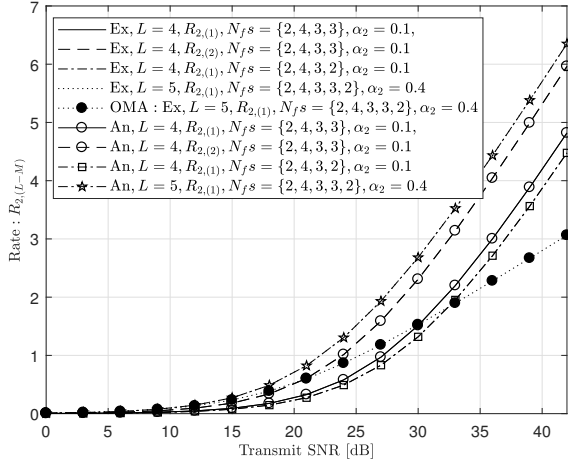


Fig. 4. Achievable rate of UE₂ for various system parameters.

cardinality of set \mathbb{S}_1 on the rate. In Fig. 5, we use fixed $|\mathbb{S}_1| = 2$ and $|\mathbb{S}_1| = 3$ for two values of L . Both underpopulated and overpopulated systems are considered. This figure shows that when the maximum value of $|\mathbb{S}_1|$ is fixed, more RRHs in \mathbb{S}_1 results in greater rate up to a certain transmit SNR. However, in the high transmit SNR region, an asymptotic rate advantage is determined by the ratio of $|\mathbb{S}_1|$ to L for underpopulated and overpopulated systems. Thus, we can observe the following results:

- $R_{1,(4,3)} > R_{1,(5,3)}$ for underpopulated system, i.e., $L \leq K$.
- $R_{1,(5,3)}$ in the system with six RRHs is greater than that of the system with seven RRHs.
- Similar results can be seen with $|\mathbb{S}_1| = 2$, i.e., $R_{1,(4,2)} > R_{1,(5,2)}$. From these observations, a greater $|\mathbb{S}_1|$ does not guarantee a greater rate in the asymptotic transmit SNR region.

A few more observations can be made from Fig. 6, which uses fixed values of $\alpha_1 = 0.7$ and $N_g s = N_f s =$

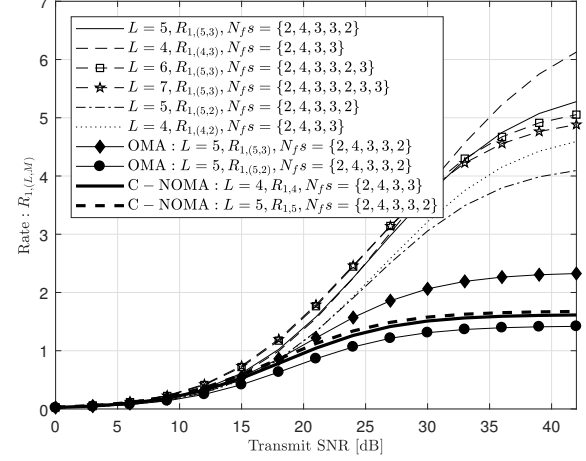


Fig. 5. Achievable rate of UE₁ for various pairs of (L, M) s in underpopulated and overpopulated systems.

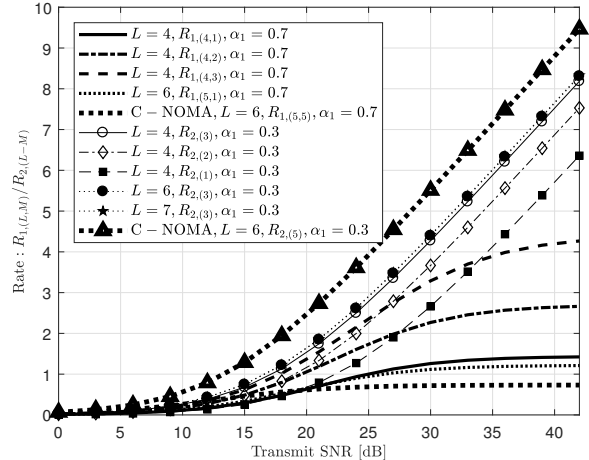


Fig. 6. Achievable rate of UE₁ and UE₂ for various values of $|\mathbb{S}_2|$ in underpopulated and overpopulated systems.

$\{2, 4, 3, 3\}$ for the underpopulated system, and $N_g s = N_f s = \{2, 4, 3, 3, 2, 3\}$, $N_g s = N_f s = \{2, 4, 3, 3, 2, 3, 3\}$, for the overpopulated system, as listed in the following:

- As $|\mathbb{S}_2|$ increases, $R_{2,(|\mathbb{S}_2|)}$ can be greater than $R_{1,(4,4-|\mathbb{S}_2|)}$.
- When $L = 4$ and $|\mathbb{S}_1| = 1$, UE₁ achieves a slightly greater rate than that of the overpopulated system with $L = 6$.
- When $|\mathbb{S}_2| = 3$, UE₂ can achieve a slightly greater rate as the system is more populated, that is, L increases.
- For this considered scenario, $R_{2,(3)}$ can be greater than $R_{1,(4,1)}$ in the underpopulated system and $R_{1,(5,1)}$ in the overpopulated system over the considered whole SNR range.
- In general, at a fixed value of α_1 , a greater $|\mathbb{S}_1|$ results in a greater achievable rate of UE₁.

b) *The impact of the number of multipath components:* In Fig. 7, we also investigate the impact of the multipath compo-

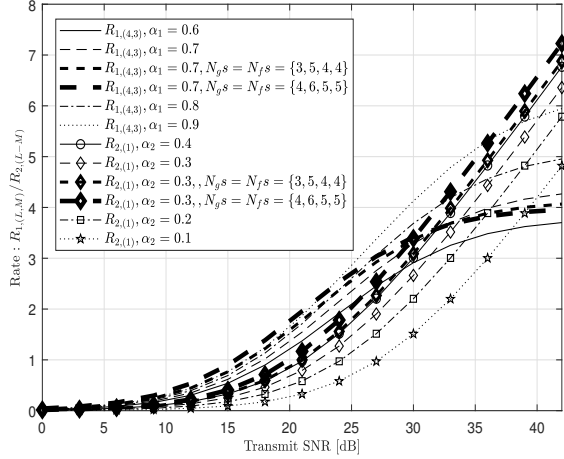


Fig. 7. Achievable rate of UE₁ and UE₂ for various values of α_1 s with $N_g s = N_f s = \{2, 4, 3, 3\}$, $L = 4$, and $|S_1| = 3$.

nents on the rate. Comparing with the reference scenario with $N_g s = N_f s = \{2, 4, 3, 3\}$, we also consider two cases with $N_g s = N_f s = \{3, 5, 4, 4\}$ and $N_g s = N_f s = \{4, 6, 5, 5\}$. Since the SNR decoding s_1 by UE₁ is related with the ratio of C_{\max}^M to D_{\min}^{L-M} , each of which increases as $N_g s$ increases, the rate of UE₁ is less affected when the number of multipath components of the channels connected to UE₁ are all simultaneously increased. However, the rate of UE₂ is increased since the SNR decoding s_2 is increased.

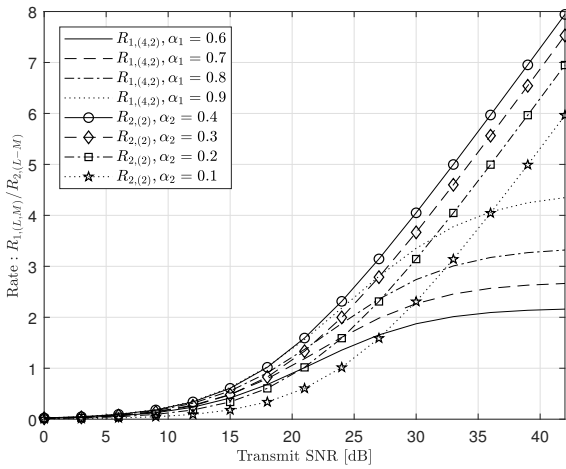


Fig. 8. Achievable rate of UE₁ and UE₂ for various values of α_1 s with $N_g s = N_f s = \{2, 4, 3, 3\}$, $L = 4$, and $|S_1| = 2$.

c) *The impact of power allocation to RRHs specified by S_1 and S_2 :* For four RRHs and $|S_1| = 3$, we investigate the impact of α_1 on the rates of UE₁ and UE₂ in Fig. 7. In this scenario, only one RRH out of four RRHs is used to transmit s_2 . This figure shows that as α_1 increases, UE₁ achieves a greater rate, whereas UE₂ achieve a lower rate since a less power is allocated to RRHs specified by S_2 . This figure also shows that $R_{2,(L-M)}$ increases as the transmit SNR increases, whereas $R_{1,(L,M)}$ is upper bounded by its

limit since γ_{1,s_1} is approximated by $\gamma_{1,s_1} \approx \frac{\alpha_1 C_{\max}^M}{\alpha_2 D_{\min}^{L-M}}$ as the transmit SNR increases. That is, UE₁ enters the interference-limited region. From these observations, the sum rate is like a double-edged sword. If the pair of (L, M) and the power allocation are not properly handled, the sum rate will be dominated by UE₂, which violates the near-far user pairing constraint. Since the CU knows only \mathbb{X}_g and controls α_1 , every pair of (L, M) is not possible to meet this constraint. For $|S_1| = 2$, i.e., two RRHs are assigned to transmit s_2 , we can see distinctive results in Fig. 8 comparing with Fig. 7. For the considered scenario, $(L = 4, M = 2, \alpha_1 = 0.6)$ and $(L = 4, M = 2, \alpha_1 = 0.7)$ are not feasible near-far user pairs. Although other pairs $(L = 4, M = 2, \alpha_1 = 0.8)$ and $(L = 4, M = 2, \alpha_1 = 0.9)$ are feasible, they have limited operating SNR ranges to support the near-far user pairing.

However, when we mainly focus on the rate of UE₁, Figs. 6, 7, and 8 suggest the following RRH assignment and power allocation scheme:

- A larger $|S_1|$ results in $R_{1,(L,M)} > R_{2,(L-M)}$, so that it is necessary to assign more RRHs to transmit s_1 . Since only a partial CSIT is available at the CU, the value of M is determined in such a way that $M > \lceil L/2 \rceil$. In addition, as α_1 decreases, it is required that $M \rightarrow L-1$, that is, only one RRH is assigned to transmit s_2 .
- Due to the existence of the interfering signal at UE₁, the CU needs to assign more transmit power to the RRHs specified by S_1 .

In the next, we will investigate another case, in which we consider UE₁ and UE₂ simultaneously under the near-far user pairing constraint.

D. Optimum sum rate

When perfect CSIT and locations of the RRHs and two users are available at the CU⁶, the following optimization can be achieved by maximizing the sum rate as follows:

$$\begin{aligned} \max_{\alpha_1} \quad & R_{1,(L,M)}(\alpha_1) + R_{2,(L-M)}(1 - \alpha_1) \\ \text{s.t.} \quad & R_{1,(L,M)}(\alpha_1) > R_{2,(L-M)}(1 - \alpha_1) \\ & 0.5 < \alpha_1 < 1.0. \end{aligned} \quad (21)$$

In generating Figs. 9 and 10, we use $N_g s = N_f s = \{2, 4, 3, 3\}$ for $L = 4$ and $N_g s = N_f s = \{2, 4, 3, 3, 2\}$ for $L = 5$. These two figures also show a feasible set of α_1 s supporting the near-far user pairing constraint. From Fig. 9 we can observe the following results:

- As $|S_1|$ decreases, the size of the feasible set α_1 s decreases as the transmit SNR increases. The near-far user pairing constraint is the key factor that determines this result.
- As the transmit SNR increases, the optimum sum rate is determined by $|S_1| = 3$.

Similarly, we can observe the following results from Fig. 10.

- As L increases, the cardinality of S_1 does not provide the optimum sum rate.

⁶Note that this is not possible from the proposed dCDD scheme.

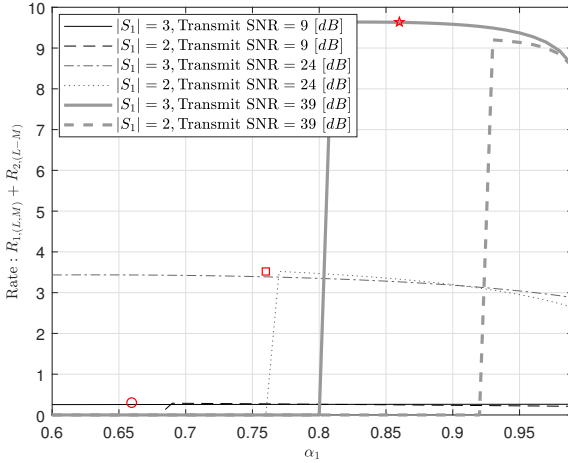


Fig. 9. Optimum sum rate, $R_{1,(L,M)}(\alpha_1) + R_{2,(L-M)}(1-\alpha_1)$, for various values of α_1 s. Three markers denote the optimum sum rate.

- As $|S_1|$ decreases, the size of the feasible set α_1 s decreases, which is similar to that of Fig. 9.
- When we compare the optimum sum rate with the scheme with $|S_1| = L - 1$ and $\alpha_1 = 0.87$, the differences are (0.0139, 0.4719, 0.1005) respectively at 9, 24, and 39 dB transmit SNRs.

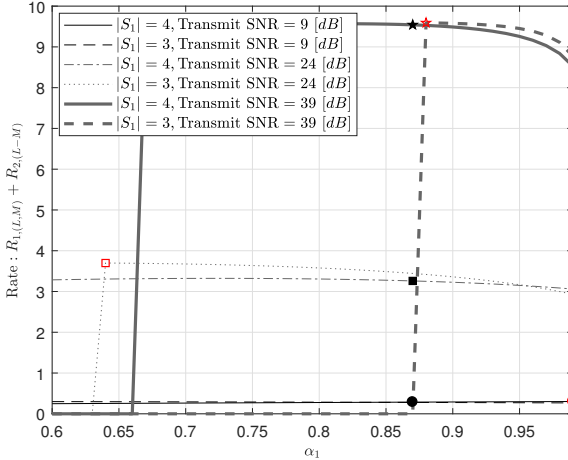


Fig. 10. Optimum sum rate, $R_{1,(L,M)}(\alpha_1) + R_{2,(L-M)}(1-\alpha_1)$, for various values of α_1 s. Three markers denote the optimum sum rate, whereas three filled markers denote the sum rate achieved by $|S_1| = L - 1$ and $\alpha_1 = 0.87$.

Based on Figs. 8-10, we propose the RRH assignment and power allocation scheme for dCDD based NOMA, with $|S_1| = L - 1$ and $\alpha_1 = 0.87$. In generating Fig. 11, we consider two scenarios: one scenario with the same channel parameters as those of Figs. 9-10, and the other scenario with $N_{gs} = N_{fs} = \{5, 4, 3, 4, 2\}$. Fig. 11 shows the following results:

- Without perfect CSIT and locations of the RRHs and two users, the proposed dCDD can achieve almost the same sum rate as that of the ideal scheme which has perfect CSIT.

- As the transmit SNR increases, the difference between two schemes becomes negligible.
- The performance gap is almost irrespective of the number of multipath components of the whole channel.

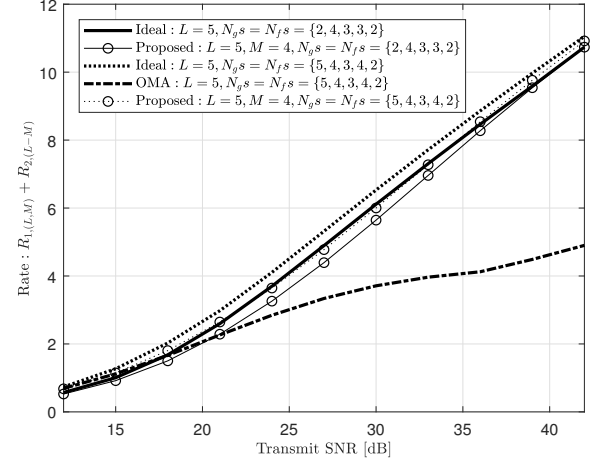


Fig. 11. Achievable sum rate for various system parameters.

E. Rate comparison with respect to dCDD-OMA and dCDD-C-NOMA

For comparison, we integrate dCDD with the traditional OMA [47, Chapter 6.2], i.e., dCDD-OMA. The same near-far user pairing is also applied to dCDD-OMA. From Figs. 4, 5, 6, and 11, we can observe that

- Although a similar trend can be identified in both schemes as the transmit SNR increases, dCDD-NOMA provides a greater rate to both users comparing with dCDD-OMA.
- Comparing with the largest sum rate achieved by dCDD-OMA, a significant improvement can be achieved by dCDD-NOMA. For example, at 4 bps/Hz, a more than 10 dB gain in terms of the transmit SNR can be achieved. As the transmit SNR increases, the performance gain increases.
- The proposed dCDD-Pseudo-NOMA assigns more RRHs to transmit s_1 and more transmit power to the RRHs indexed by the set S_1 . These two conditions are required to satisfy the near-far user pairing constraint. Although the rate of UE₁ is mainly influenced by these two conditions, UE₂ also benefits from joint transmissions. However, dCDD-C-NOMA makes only UE₂ benefited from joint transmissions. Thus, a greater sum rate can be achieved by the proposed dCDD-Pseudo-NOMA comparing with dCDD-C-NOMA. From the derived receive SNRs, which are respectively expressed by γ_{2,s_1} and γ_{2,s_2} , we can expect these results. Since there is no feasible region of $R_{1,(L,L)} > R_{2,(L)}$ for dCDD-C-NOMA, the achievable sum rate is not included in Fig. 11.

F. Achievable rate for three users

The following setup is used to justify the extension of the proposed dCDD-Pseudo-NOMA into three users cases.

- With $B = 96$ and $N_{CP} = 8$, twelve RRHs can be supported by dCDD operation.
- Twelve RRHs are placed at $\{(0, 12), (-12, 12), (-3, 12), (-9, 12), (-16.9145, 6.1564), (-6, 8), (-12, 10), (-10, 9.4), (-7, 8.7), (-9.3, 9.7), (-4.3, 5.7), (-1.3, 8.4)\}$ in a 2-D plane.
- The three users, UE₁, UE₂, and UE₃, are respectively placed at $(5, -4)$, $(3, -3)$, and $(-3, 3)$.
- A multipath channel from the m th RRH to UE₃, \mathbf{h}_m , is similarly defined as \mathbf{f}_m with $N_{h,m} \triangleq |\mathbf{h}_m|$ multipath components.
- We assume $N_{fs} = \{2, 3, 4, 3, 2, 2, 3, 3, 2, 2, 3, 3\}$ and $N_{gs} = N_{hs} = \{4, 6, 6, 5, 4, 4, 5, 4, 3, 5, 4, 5\}$.

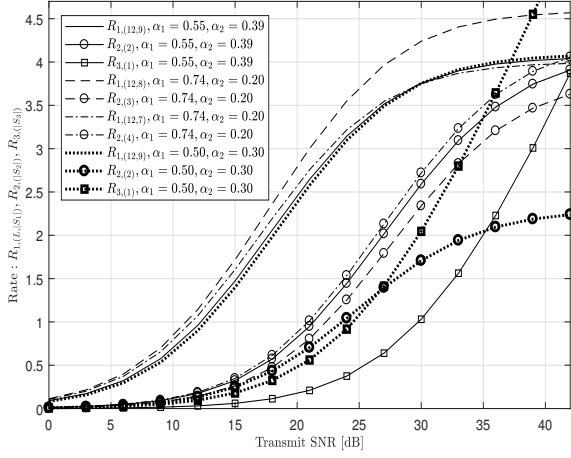


Fig. 12. Achievable rate of UE₁, UE₂, and UE₃ for various values of $(\alpha_1, \alpha_2, \alpha_3 = 1 - \alpha_1 - \alpha_2)$, $(|S_1|, |S_2|, |S_3|)$, and $(K = L = 12)$.

Fig. 12 provides the following results for the full-populated system, i.e., $K = L$:

- In contrast to the two users case, a more number of RRHs is required to support more than two users.
- As in the two users case, only a small number of RRHs is required to transmit the signals targeting at the nearest user satisfying near-far user pairing constraint.
- In general, as the number of RRHs for dCDD increases, α_2 can be increased. However, it should be less than α_1 .
- When we compare the case ($|S_1| = 9, |S_2| = 2, |S_3| = 1, \alpha_1 = 0.50, \alpha_2 = 0.30$) with ($|S_1| = 9, |S_2| = 2, |S_3| = 1, \alpha_1 = 0.55, \alpha_2 = 0.39$), it is necessary to consider more tight restriction on choosing α_2 and ($|S_1|, |S_2|, |S_3|$). Especially, when we choose ($|S_1| = 9, |S_2| = 2, |S_3| = 1, \alpha_1 = 0.50, \alpha_2 = 0.30$), the operating SNR is only up to 27 dB by near-far user pairing constraint.

V. CONCLUSIONS AND FUTURE WORKS

In this paper, we have proposed a new transmit diversity scheme for the two-user CP-SC Pseudo-NOMA system. To support the near-far user pairing, a new joint RRH assignment and power allocation scheme for dCDD-based CP-SC transmissions to achieve transmit diversity for downlink NOMA systems has been proposed without requiring perfect CSIT of

the whole channels at the CU. For i.n.i.d. frequency selective fading channels, new closed-form expressions for rate of two users have been derived. Its accuracy has also been verified. The proposed RRH assignment and power allocation scheme, that uses as many as RRHs to transmit the information signal to the far user and allocates as much as transmit power to transmit this signal, can achieve almost the same rate as that of the ideal system. As the transmit SNR increases, a difference in the sum of rate has been shown to be decreased, and irrespective of the number of multipath components of the whole channel. Extension to the system that supports multi-clusters, each of which is composed of two users, will be one of the future works.

APPENDIX A: DERIVATION OF Corollary 1

The PDF of the RV A can be derived as follows:

$$f_A(y) = \sum_{i_1=L-M+1}^L \sum_{j_1=1}^{L_{f,i_1}} Pr_{i_1} \theta_{L,M}(i_1, j_1) (y)^{j_1-1} e^{-\beta_{2,i_1} y} / \Gamma(j_1) \quad (\text{A.1})$$

where $\theta_{L,M}(i_1, j_1) \triangleq \frac{\partial^{N_{f,i_1}-j_1}}{\partial s^{N_{f,i_1}-j_1}} ((s + \beta_{2,i_1})^{N_{f,i_1}} \prod_{n=L-M+1}^L (s + \beta_{2,n})^{-N_{f,n}})|_{s=-\beta_{2,i_1}} \frac{\prod_{i=1}^L (\beta_{2,i})^{N_{f,i}}}{\Gamma(N_{f,i_1} - j_1 + 1)}$. Similarly the density function of the RV B can be derived as follows:

$$f_B(y) = \sum_{i_2=1}^{L-M} \sum_{j_2=1}^{L_{f,i_2}} Pr_{i_2} \theta_{L,L-M}(i_2, j_2) (y)^{j_2-1} e^{-\beta_{2,i_2} y} / \Gamma(j_2) \quad (\text{A.2})$$

where $\theta_{L,L-M}(i_2, j_2) \triangleq \frac{\partial^{N_{f,i_2}-j_2}}{\partial s^{N_{f,i_2}-j_2}} ((s + \beta_{2,i_2})^{N_{f,i_2}} \prod_{n=1}^{L-M} (s + \beta_{2,n})^{-N_{f,n}})|_{s=-\beta_{2,i_2}} \frac{\prod_{i=1}^{L-M} (\beta_{2,i})^{N_{f,i}}}{\Gamma(N_{f,i_2} - j_2 + 1)}$. Using Eqs. (A.1) and (A.2), the PDF of γ_{2,s_1} is derived as follows:

$$\begin{aligned} f_{\gamma_{2,s_1}}(x) &= \int_0^\infty ((\alpha_2 y + 1)/\alpha_1) f_A(x(\alpha_2 y + 1)/\alpha_1) f_B(y) dy \\ &\propto (\alpha_1)^{-j_1} \sum_{l=0}^{j_1} \binom{j_1}{l} (\alpha_2)^l \Gamma(l + j_2) e^{-(\beta_{2,i_1}/\alpha_1)x} x^{j_1-1} \\ &\quad ((\alpha_2 \beta_{2,i_1})/\alpha_1)x + \beta_{2,i_2})^{-l-j_2}. \end{aligned} \quad (\text{A.3})$$

According to (A.3), we can have (4).

APPENDIX B: DERIVATION OF Corollary 2

With the condition $0 < \tilde{\lambda}_{n_1} < \tilde{\lambda}_{n_2} < \dots < \dots < \tilde{\lambda}_{n_{L_1}} < \infty$, $Pr_{\{n_1, \dots, n_{L_1}\} \in S_2}$ is given by

$$Pr_{\{n_1, \dots, n_{L_1}\} \in S_2} = \int_0^\infty f_{\tilde{\lambda}_{n_1}}(x) \left[\prod_{i=2}^{L_1} F_{\tilde{\lambda}_{n_i}}(x) \right]_{J_2} \left[\prod_{j=L_1+1}^L (1 - F_{\tilde{\lambda}_{n_j}}(x)) \right]_{J_3} dx \quad (\text{B.1})$$

where $F_{\tilde{\lambda}_{n_i}}(x)$ can be expressed as follows:

$$F_{\tilde{\lambda}_{n_i}}(x) = \sum_{k_{i,1}, \dots, k_{i,N_{g,n_i}+1}} \binom{1}{k_{i,1}, \dots, k_{i,N_{g,n_i}+1}} (-1)^{r_{n_i}} (\beta_{1,n_i})^{\eta_{n_i}} (\theta_{n_i})^{-1} x^{\eta_{n_i}} e^{-\beta_{1,n_i} r_{n_i} x}. \quad (\text{B.2})$$

With the use of the multinomial theorem [48], r_{n_i} , η_{n_i} , and θ_{n_i} are defined as follows:

$$\begin{aligned} r_{n_i} &\stackrel{\Delta}{=} \sum_{l=2}^{N_{g,n_i}+1} k_{i,l}, \quad \eta_{n_i} \stackrel{\Delta}{=} \sum_{l=3}^{N_{g,n_i}+1} (l-2)k_{i,l}, \text{ and} \\ \theta_{n_i} &\stackrel{\Delta}{=} \prod_{l=2}^{N_{g,n_i}} (\Gamma(l))^{k_{i,l+1}}. \end{aligned} \quad (\text{B.3})$$

Thus, $[\cdot]_{J_2}$ can be evaluated as follows:

$$[\cdot]_{J_2} = \Psi x^{(\sum_{i=2}^{L_1} \eta_{n_i})} e^{-(\sum_{i=2}^{L_1} \beta_{1,n_i} r_{n_i})x} \quad (\text{B.4})$$

with $\Psi \stackrel{\Delta}{=} \sum_{\substack{k_{1,1}, \dots, k_{1,N_{g,n_1}+1} \\ k_{1,1} + \dots + k_{1,N_{g,n_1}+1} = 1}} \dots \sum_{\substack{k_{L_1,1}, \dots, k_{L_1,N_{g,n_{L_1}+1}} \\ k_{L_1,1} + \dots + k_{L_1,N_{g,n_{L_1}+1}} = 1}} \prod_{i=2}^{L_1} \left(\frac{(-1)^{r_{n_i}} (\beta_{1,n_i})^{\eta_{n_i}}}{\theta_{n_i}} \right)$. Similarly, $[\cdot]_{J_3}$ can be evaluated as follows:

$$[\cdot]_{J_3} = \Phi x^{(\sum_{j=L_1+1}^L l_{n_j})} e^{-(\sum_{j=L_1+1}^L \beta_{1,n_j})x} \quad (\text{B.5})$$

with $\Phi \stackrel{\Delta}{=} \sum_{l_{n_{L_1+1}}=0}^{N_{g,n_{L_1+1}}-1} \dots \sum_{l_{n_L}=0}^{N_{g,n_L}-1} \prod_{j=L_1+1}^L \left(\frac{(\beta_{1,n_j})^{l_{n_j}}}{\Gamma(l_{n_j}+1)} \right)$. Having used (B.4) and (B.5), (B.1) can be derived as (10).

APPENDIX C: DERIVATION OF Corollary 3

When $|\mathbb{S}_2| = 1$, $Pr_{m \in \mathbb{S}_2}$ is computed as follows:

$$Pr_{m \in \mathbb{S}_2} = \int_0^\infty f_{\tilde{\lambda}_m}(x) \prod_{k=1, k \neq m}^L (1 - F_{\tilde{\lambda}_k}(x)) dx \quad (\text{C.1})$$

where $\tilde{\lambda}_m \stackrel{\Delta}{=} \|g_m\|^2 / \beta_{1,m}$. The PDF and CDF of $\tilde{\lambda}_m$ are respectively given by

$$\begin{aligned} f_{\tilde{\lambda}_m}(x) &= (\beta_{1,m})^{N_{g,m}} x^{N_{g,m}-1} e^{-\beta_{1,m}x} / \Gamma(N_{g,m}) \text{ and} \\ F_{\tilde{\lambda}_m}(x) &= \Gamma_U(N_{g,m}, \beta_{1,m}x) / \Gamma(N_{g,m}) \end{aligned} \quad (\text{C.2})$$

where $\Gamma_U(\cdot, \cdot)$ denotes the incomplete upper-gamma function [48]. Thus, (C.1) is given by

$$Pr_{m \in \mathbb{S}_2} = (\beta_{1,m})^{N_{g,m}} \Phi_1 \int_0^\infty x^{\sum_{k=1, k \neq m}^L l_k + N_{g,m}-1} e^{-\sum_{k=1}^L \beta_{1,k}x} / \Gamma(N_{g,m}) dx \quad (\text{C.3})$$

with $\Phi_1 \stackrel{\Delta}{=} \sum_{\{l_1, \dots, l_L\} \setminus \{l_m\}}^{\{N_{g,1}-1, \dots, N_{g,L}-1\} \setminus \{N_{g,m}-1\}} \left(\prod_{k=1, k \neq m}^L \frac{(\beta_{1,k})^{l_k}}{\Gamma(l_k+1)} \right)$. After some manipulations, we can readily derive (12).

APPENDIX D: DERIVATION OF Corollary 4

When m and n are elements of \mathbb{S}_2 , i.e., $|\mathbb{S}_2| = 2$, then $Pr_{\{m,n\} \in \mathbb{S}_2}$ with the condition $0 < \tilde{\lambda}_m < \tilde{\lambda}_n < \infty$ is given by

$$\begin{aligned} Pr_{\{m,n\} \in \mathbb{S}_2} &= \int_0^\infty f_{\tilde{\lambda}_n}(x) F_{\tilde{\lambda}_m}(x) \\ &\quad \left[\prod_{k=1, k \neq \{m,n\}}^L (1 - F_{\tilde{\lambda}_k}(x)) \right]_{J_4} dx \end{aligned} \quad (\text{D.1})$$

where $F_{\tilde{\lambda}_m}(x)$ can be expressed as follows:

$$\begin{aligned} F_{\tilde{\lambda}_m}(x) &= \sum_{\substack{k_1, \dots, k_{N_{g,m}+1} \\ k_1 + \dots + k_{N_{g,m}+1} = 1}} \binom{1}{k_1, \dots, k_{N_{g,m}+1}} \\ &\quad (-1)^{r_m} (\beta_{1,m})^{\eta_m} (\theta_m)^{-1} x^{\eta_m} e^{-\beta_{1,m}r_m x} \\ &= \Psi_2 x^{\eta_m} e^{-\beta_{1,m}r_m x}. \end{aligned} \quad (\text{D.2})$$

Due to the use of the multinomial theorem [48], we define the following terms:

$$\begin{aligned} r_m &\stackrel{\Delta}{=} \sum_{l=2}^{N_{g,m}+1} k_l, \quad \eta_m \stackrel{\Delta}{=} \sum_{l=3}^{N_{g,m}+1} (l-2)k_l, \text{ and} \\ \theta_m &\stackrel{\Delta}{=} \prod_{l=2}^{N_{g,m}} (\Gamma(l))^{k_{l+1}}. \end{aligned} \quad (\text{D.3})$$

Furthermore, $[\cdot]_{J_4}$ is given by

$$[\cdot]_{J_4} = \Phi_2 x^{(\sum_{k=1, k \neq \{m,n\}}^L l_k)} e^{-(\sum_{k=1, k \neq \{m,n\}}^L \beta_{1,k})x} \quad (\text{D.4})$$

where $\Phi_2 \stackrel{\Delta}{=} \sum_{\{l_1, \dots, l_L\} \setminus \{l_m, l_n\}}^{\{N_{g,1}-1, \dots, N_{g,L}-1\} \setminus \{N_{g,m}-1, N_{g,n}-1\}} \left(\prod_{k=1, k \neq \{m,n\}}^L \frac{(\beta_{1,k})^{l_k}}{\Gamma(l_k+1)} \right)$. Having applied (D.4) along with (D.2) into (D.1), we can readily derive (14).

APPENDIX E: DERIVATION OF Corollary 5

Recall that X_k is the k th smallest instantaneous SNR. Its complementary CDF (CCDF) and PDF are respectively defined as follows:

$$\begin{aligned} \tilde{F}_{X_k}(x_k) &= \Gamma_U(N_{g,k}, \beta_{1,k}x_k) / \Gamma(N_{g,k}) \text{ and} \\ f_{X_k}(x_k) &= (\beta_{1,k})^{N_{g,k}} e^{-\beta_{1,k}x_k} (x_k)^{N_{g,k}-1} / \Gamma(N_{g,k}). \end{aligned} \quad (\text{E.1})$$

a) *Derivation of the PDF of D_{\min}^{L-M}* : The joint PDF of X_1, \dots, X_{L-M} is given by

$$\begin{aligned} f_{X_1, \dots, X_{L-M}}(x_1, \dots, x_{L-M}) &= \\ \sum_{\substack{n_1, \dots, n_{L-M} \\ n_1 \neq n_2 \neq \dots \neq n_{L-M}}}^L &\prod_{j=1}^{L-M} \frac{(\beta_{n_j})^{m_{n_j}}}{\Gamma(m_{n_j})} (x_j)^{m_{n_j}-1} \\ \prod_{j=L-M+1}^L &\Gamma(m_{n_j}, \beta_{n_j} x_{L-M}) / \Gamma(m_{n_j}) \end{aligned} \quad (\text{E.2})$$

where $\beta_j \stackrel{\Delta}{=} \beta_{1,\langle j \rangle}$ and $m_j \stackrel{\Delta}{=} N_{g,\langle j \rangle}$. The moment generating function (MGF) of D_{\min}^{L-M} can be given by (E.3). In (E.3), $[\cdot]_J$ is given by (E.4). In (E.4), we have defined $C_2 \stackrel{\Delta}{=} \prod_{j=1}^{L-M} (\beta_{n_j})^{m_{n_j}} / \Gamma(m_{n_j})$, $C_3 \stackrel{\Delta}{=} \prod_{j=L-M+1}^L (\beta_{n_j})^{l_j} / \Gamma(l_j+1)$, $\tilde{m}_{\min} \stackrel{\Delta}{=} \sum_{j=L-M+1}^L l_j + m_{n_{L-M}} - 1$, and $\tilde{\beta}_{\min} \stackrel{\Delta}{=} \sum_{j=L-M}^L \beta_{n_j}$. Due to the dependency on preceding RVs in the lower integration limit, the computation of (E.3) is in general infeasible [16]. In addition, it is necessary to compute the distribution of the ratio of two RVs, which are correlated to each other. Thus, it is desirable to convert D_{\min}^{L-M} and C_{\max}^M into the sum of independent RVs, which will make $M_{D_{\min}^{L-M}}(s)$ the product of MGFs, each of which corresponds to an independent RV. This can be possible by using the spacing statistics of the order statistics. To obtain the spacing statistics, we apply the transformation from $\{X_1, \dots, X_{L-M}\}$ to $\{Y_1, \dots, Y_{L-M}\}$ by $Y_1 = X_1, Y_2 = X_1 + X_2, \dots, Y_{L-M} = X_1 + \dots + X_{L-M}$. For (E.4), we can have the form given by (E.5). In (E.5), we have defined $\xi_i = \frac{1}{(L-M-i+1)} \sum_{j=i}^L \beta_{n_j}$ and $\nu_i = \begin{cases} m_{n_1} - 1 + \sum_{j=2}^{L-M} p_{j,i} & \text{for } i = 1 \\ \sum_{j=i}^{L-M} p_{j,i} & \text{for } 2 \leq i \leq L-M \end{cases}$. After expanding each sum of the RVs by the multinomial theorem [48], we can obtain (E.5). Due to the transformation of continuous RVs, the lower integration limits of (E.3)

$$M_{D_{\min}^{L-M}}(s) = \sum_{n_1 \neq n_2 \neq \dots \neq n_{L-M}}^L \int_0^\infty \int_{x_1}^\infty \dots \int_{x_{L-M-2}}^\infty \int_{x_{L-M-1}}^\infty \left[\prod_{j=1}^{L-M} (\beta_{n_j})^{m_{n_j}} (x_j)^{m_{n_j}-1} / \Gamma(m_{n_j}) \right] \\ \prod_{j=L-M+1}^L \Gamma_U(m_{n_j}, \beta_{n_j} x_{L-M}) e^{-s(\sum_{j=1}^{L-M} x_j)} / \Gamma(m_{n_j}) \Big] J dx_{L-M} \dots dx_2 dx_1. \quad (\text{E.3})$$

$$[\cdot]_J = C_2 \sum_{l_{L-M+1}=0}^{m_{n_{L-M+1}}-1} \dots \sum_{l_L=0}^{m_{n_L}-1} C_3 \left(\prod_{j=1}^{L-M-1} (x_j)^{m_{n_j}-1} e^{-\beta_{n_j} x_j} \right) (x_{L-M})^{\tilde{m}_{\min}} e^{-\tilde{\beta}_{\min} x_{L-M}} e^{-s(\sum_{j=1}^{L-M} x_j)}. \quad (\text{E.4})$$

$$[\cdot]_J = C_2 \sum_{l_{L-M+1}=0}^{m_{n_{L-M+1}}-1} \dots \sum_{l_L=0}^{m_{n_L}-1} C_3 \sum_{\substack{p_{2,1}, p_{2,2} \\ \sum_{i_2=1}^2 p_{2,i_2} = m_{n_2}-1}} \frac{\Gamma(m_{n_2})}{\prod_{i=1}^2 p_{2,i}!} \dots \sum_{\substack{p_{L-M,1}, \dots, p_{L-M,L-M} \\ \sum_{i=L-M+1}^{L-M} p_{L-M,i} = \tilde{m}_{\min}}} \frac{\Gamma(\tilde{m}_{\min}+1)}{\prod_{i=1}^{L-M} p_{L-M,i}!} \\ \prod_{i=1}^{L-M} \left(x_i^{\nu_i} e^{-x_i((L-M-i+1)s+(L-M-i+1)\xi_i)} \right). \quad (\text{E.5})$$

becomes zero and they are independent of each other, so that $M_{D_{\min}^{L-M}}(s)$ can be evaluated as follows:

$$M_{D_{\min}^{L-M}}(s) = \sum_{n_1 \neq n_2 \neq \dots \neq n_{L-M}}^L \left[\prod_{i=1}^{L-M} ((s + \xi_i)^{-\nu_i-1}) \right]_{A_1} \quad (\text{E.6})$$

where $\sum_{n_1 \neq n_2 \neq \dots \neq n_{L-M}}^L \triangleq \sum_{n_1 \neq n_2 \neq \dots \neq n_{L-M}}^L C_2 \sum_{l_{L-M+1}=0}^{m_{n_{L-M+1}}-1} \dots \sum_{l_L=0}^{m_{n_L}-1} C_3 \sum_{\substack{p_{2,1}, p_{2,2} \\ \sum_{i_2=1}^2 p_{2,i_2} = m_{n_2}-1}} \frac{\Gamma(m_{n_2})}{\prod_{i=1}^2 p_{2,i}!} \dots \sum_{\substack{p_{L-M,1}, \dots, p_{L-M,L-M} \\ \sum_{i=L-M+1}^{L-M} p_{L-M,i} = \tilde{m}_{\min}}} \frac{\Gamma(\tilde{m}_{\min}+1)}{\prod_{i=1}^{L-M} p_{L-M,i}!} (L-M)^{-\nu_1-1} (L-M-1)^{-\nu_2-1} \dots 2^{-\nu_{L-M-1}-1} \Gamma(\nu_1+1) \Gamma(\nu_2+1) \dots \Gamma(\nu_{L-M-1}+1) \Gamma(\nu_{L-M}+1)$. Note that, in general, $\xi_1 \neq \xi_2 \neq \dots \neq \xi_{L-M}$. After applying the PF to A_1 in (E.6), and the inverse MGF, the PDF can be derived as follows:

$$f_{D_{\min}^{L-M}}(t) = \sum_{n_1 \neq n_2 \neq \dots \neq n_{L-M}}^L \sum_{i=1}^{L-M} \sum_{j=1}^{\nu_i+1} E_{\min^{L-M}}(i, j) e^{-\xi_i t} t^{j-1} / \Gamma(j) \quad (\text{E.7})$$

$$\text{where } E_{\min^{L-M}}(i, j) \triangleq \frac{1}{\Gamma(\nu_i-l+2)} \frac{\partial^{\nu_i+1-j}}{\partial s^{\nu_i+1-j}} ((s + \xi_i)^{\nu_i+1} \prod_{n=1}^{L-M} (s + \xi_n)^{-\nu_n-1})|_{s=-\xi_i}.$$

b) *Derivation of the PDF of C_{\max}^M :* The joint density function of $Z_1 \triangleq X_{L-M+1}, \dots, Z_M \triangleq X_L$ can be written as

$$f_{Z_1, \dots, Z_M}(z_1, \dots, z_M) = \sum_{n_1 \neq n_2 \neq \dots \neq n_M}^L \left[\prod_{k=1}^M f_{Z_{n_k}}(z_k) \prod_{k=M+1}^L F_{Z_{n_k}}(z_1) \right]_{J_5} \quad (\text{E.8})$$

where $F_{Z_{n_k}}(z_k) = \frac{\gamma_l(N_{g,L-M+n_k}, \beta_{1,L-M+n_k} z_k)}{\Gamma(N_{g,L-M+n_k})}$, with $\gamma_l(\cdot, \cdot)$ denoting incomplete lower-gamma function. To simplify notation, we use $\tilde{n}_k \triangleq L - M + n_k$ in the sequel. The MGF of C_{\max}^M can be defined as

$$M_{C_{\max}^M}(s) = \sum_{n_1 \neq n_2 \neq \dots \neq n_M}^L \int_0^\infty \int_{z_1}^\infty \dots \int_{z_{M-2}}^\infty \int_{z_{M-1}}^\infty [\cdot]_{J_5} dz_M \dots dz_2 dz_1 \quad (\text{E.9})$$

where $[\cdot]_{J_5}$ can be expressed as follows:

$$[\cdot]_{J_5} = D_1 D_2 (z_1)^{\tilde{m}_{\max}} e^{-z_1(s+\sum_{i=1}^M \beta_{\tilde{n}_i} + \sum_{i=M+1}^L \beta_{\tilde{n}_i} q_i)} \left(\prod_{i=2}^M (z_i)^{m_{n_i}-1} e^{-z_i(s+\beta_{\tilde{n}_i})} \right) \quad (\text{E.10})$$

where $D_1 \triangleq \prod_{j=1}^M (\beta_{n_j})^{m_{n_j}} / \Gamma(m_{n_j})$, $\tilde{k}_l \triangleq \sum_{t=0}^{m_{n_l}-1} t k_{l,t+1}$, $\tilde{m}_{\max} \triangleq m_{n_1}-1 + \sum_{l=M+1}^L \tilde{k}_l$, and $D_2 \triangleq (\prod_{j=M+1}^L C_{q_j})$ with

$$C_{q_j} \triangleq \sum_{q_j=0}^1 (-1)^{q_j} \sum_{\substack{k_{j,1}, \dots, k_{j,m_{n_j}} \\ k_{j,1} + \dots + k_{j,m_{n_j}} = 1}} \frac{1}{k_{j,1}! \dots k_{j,m_{n_j}}!} \\ \prod_{t=0}^{m_{n_j}-1} (\beta_{n_j})^{k_{j,t+1}} / (t!). \quad (\text{E.11})$$

In the derivation of (E.10), binomial and multinomial theorems [48] are used. We also use the spacing statistics, that is, $Y_1 = Z_1$ and $Y_{k \geq 2} = \sum_{j=1}^K Z_k$. Then, we can have an alternative expression for $[\cdot]_{J_5}$ is given by (E.12). In (E.12), we have defined $\zeta_i = \begin{cases} \frac{1}{M} (\sum_{j=1}^M \beta_{\tilde{n}_j} + \sum_{j=M+1}^L \beta_{\tilde{n}_j} q_j) & \text{for } i = 1 \\ \frac{1}{(M-i+1)} \sum_{j=i}^M \beta_{\tilde{n}_j} & \text{for } 2 \leq i \leq M, \end{cases}$, $\mu_i = \begin{cases} \tilde{m}_{\max} + \sum_{j=2}^M q_{j,1} & \text{for } i = 1 \\ \sum_{j=i}^M p_{j,i} & \text{for } 2 \leq i \leq M \end{cases}$. Since $y_{j,i}$ are independent of each other and lower integration limits are zero, it is possible to integrate separately. Thus, the MGF can be derived as (E.13). where $D_3 \triangleq (M)^{-\mu_1-1} (M-1)^{-\mu_2-1} \dots 2^{-\mu_{M-1}-1} \Gamma(\mu_1+1) \dots \Gamma(\mu_M+1)$. Note that $\zeta_i \neq \zeta_j$ for $\forall i, j$ with $i \neq j$. Thus, after applying the PF to $[\cdot]_{A_2}$ and then the inverse MGF, the PDF can be derived as follows:

$$f_{C_{\max}^M}(t) = \sum_{n_1 \neq n_2 \neq \dots \neq n_M}^L \sum_{i=1}^M \sum_{j=1}^{\mu_i+1} E_{\max^M}(i, j) e^{-\zeta_i t} t^{j-1} / \Gamma(j) \quad (\text{E.14})$$

$$\text{where } \sum_{n_1 \neq n_2 \neq \dots \neq n_M}^L \triangleq D_1 D_2 \sum_{\substack{p_{2,1}, p_{2,2} \\ \sum_{i=1}^2 p_{2,i} = m_{n_2}-1}} \frac{\Gamma(m_{n_2})}{\prod_{i=1}^2 p_{2,i}!} \dots \sum_{\substack{p_{3,1}, p_{3,2}, p_{3,3} \\ \sum_{i=1}^3 p_{3,i} = m_{n_3}-1}} \frac{\Gamma(m_{n_3})}{\prod_{i=1}^3 p_{3,i}!} \dots \sum_{\substack{p_{M,1}, \dots, p_{M,M} \\ \sum_{i=1}^M p_{M,i} = m_{n_M}-1}} \frac{\Gamma(m_{n_M})}{\prod_{i=1}^M p_{M,i}!}$$

$$[\cdot]_{J_5} = D_1 D_2 \sum_{\substack{p_{2,1}, p_{2,2} \\ p_{2,1} + p_{2,2} = m_{n_2} - 1}} \frac{\Gamma(m_{n_2})}{\prod_{i=1}^2 p_{2,i}!} \sum_{\substack{p_{3,1}, p_{3,2}, p_{3,3} \\ p_{3,1} + p_{3,2} + p_{3,3} = m_{n_3} - 1}} \frac{\Gamma(m_{n_3})}{\prod_{i=1}^3 p_{3,i}!} \cdots \\ \sum_{\substack{p_{M,1}, \dots, p_{M,M} \\ p_{M,1} + \dots + p_{M,M} = m_{n_M} - 1}} \frac{\Gamma(m_{n_M})}{\prod_{i=1}^M p_{M,i}!} \left(\prod_{i=1}^M y_i^{\mu_i} e^{-y_i((M-i+1)(s+\zeta_i))} \right). \quad (\text{E.12})$$

$$M_{C_{\max}^M}(s) = \sum_{\substack{n_1, \dots, n_M \\ n_1 \neq n_2 \neq \dots \neq n_M}}^L D_1 D_2 \sum_{\substack{p_{2,1}, p_{2,2} \\ p_{2,1} + p_{2,2} = m_{n_2} - 1}} \frac{\Gamma(m_{n_2})}{\prod_{i=1}^2 p_{2,i}!} \sum_{\substack{p_{3,1}, p_{3,2}, p_{3,3} \\ p_{3,1} + p_{3,2} + p_{3,3} = m_{n_3} - 1}} \frac{\Gamma(m_{n_3})}{\prod_{i=1}^3 p_{3,i}!} \\ \cdots \sum_{\substack{p_{M,1}, \dots, p_{M,M} \\ p_{M,1} + \dots + p_{M,M} = m_{n_M} - 1}} \frac{\Gamma(m_{n_M})}{\prod_{i=1}^M p_{M,i}!} D_3 \left[\prod_{i=1}^M (s + \zeta_i)^{-\mu_i - 1} \right]_{A_2}. \quad (\text{E.13})$$

$$\frac{\Gamma(m_{n_M})}{\prod_{i=1}^M p_{M,i}!} D_3, \text{ and } E_{\max M}(i,j) \stackrel{\Delta}{=} \prod_{l=1}^M \frac{1}{\Gamma(\mu_l - l + 2)} \frac{\partial^{\mu_l + 1 - j}}{\partial s^{\mu_l + 1 - j}} \\ ((s + \zeta_i)^{\mu_i + 1} \prod_{n=1}^M (s + \zeta_n)^{-\mu_n - 1})|_{s=-\zeta_i}.$$

APPENDIX F: DERIVATION OF Theorem 1

The rate, $R_{1,(M,L-M)}$, is given by

$$R_{1,(M,L-M)} = \int_0^\infty \log_2(1+x) f_{\gamma_{1,s_1}}(x) dx. \quad (\text{F.1})$$

To compute (F.1), we first express the following functions of x in terms of Meijer G-functions [43]:

$$\begin{aligned} \log_2(1+x)x^{j_4-1} &= (\log(2))^{-1} G_{2,2}^{1,2}(x| \begin{array}{c} j_4, j_4 \\ j_4, j_4 - 1 \end{array}), \\ e^{-(\zeta_{i_4}/\alpha_1)x} &= G_{0,1}^{1,0}((\zeta_{i_4}/\alpha_1)x| \begin{array}{c} \cdot \\ 0 \end{array}), \text{ and} \\ ((\alpha_2 \zeta_{i_4}/\alpha_1)x + \xi_{j_3})^{-l-j_3} &= G_{1,1}^{1,1}\left(\frac{\alpha_2 \zeta_{i_4}}{\alpha_1 \xi_{j_3}}x| \begin{array}{c} 1-l-j_3 \\ 0 \end{array}\right) \\ &\quad (\xi_{j_3})^{-l-j_3}. \end{aligned} \quad (\text{F.2})$$

Having applied [49], we can derive (20).

REFERENCES

- [1] K. J. Kim, H. Liu, H. Lei, Z. Ding, P. Orlik, and H. V. Poor, "A dCDD-Based transmit diversity for NOMA systems," in *Proc. IEEE Int. Conf. Commun.*, Dublin, Ireland, Jun. 2020.
- [2] S. M. R. Islam, N. Avazov, O. A. Dobre, and K. Kwak, "Power-domain non-orthogonal multiple access (NOMA) in 5G systems: Potentials and challenges," *IEEE Commun. Surveys Tuts.*, vol. 19, no. 2, pp. 721–742, 2017.
- [3] L. Dai, B. Wang, Y. Yuan, S. Han, C.-L. I, and Z. Wang, "Non-orthogonal multiple access for 5G: solutions, challenges, opportunities, and future research trends," *IEEE Commun. Mag.*, pp. 74–81, Sep. 2015.
- [4] Z. Ding, Y. Liu, J. Choi, Q. Sun, M. Elkashlan, I. C. L, and H. V. Poor, "Application of non-orthogonal multiple access in LTE and 5G networks," *IEEE Commun. Mag.*, pp. 185–191, Feb. 2017.
- [5] Z. Ding, X. Lei, G. K. Karagiannidis, R. Schober, J. Yuan, and V. K. Bhargava, "A survey on non-orthogonal multiple access for 5G networks: Research challenges and future trends," *IEEE J. Sel. Areas Commun.*, vol. 35, no. 10, pp. 2181–2195, Oct. 2017.
- [6] Z. Ding, F. Adachi, and H. V. Poor, "The application of MIMO to non-orthogonal multiple access," *IEEE Trans. Wireless Commun.*, vol. 15, no. 1, pp. 537–552, Jan. 2016.
- [7] Z. Ding, P. Fan, and H. V. Poor, "Impact of user pairing on 5G non-orthogonal multiple-access downlink transmissions," *IEEE Trans. Veh. Technol.*, vol. 65, no. 8, pp. 6010–6023, 2016.
- [8] Z. Ding, R. Schober, and H. V. Poor, "A general MIMO framework for NOMA downlink and uplink transmission based on signal alignment," *IEEE Trans. Wireless Commun.*, vol. 15, no. 6, pp. 4438–4454, Jun. 2016.
- [9] E. Balevi, "Multiuser diversity gain in uplink NOMA," in *Proc. 2018 IEEE Vehicular Technology Conference (VTC-Fall)*, Chicago, IL, 27-30 Aug. 2018, pp. 1–5.
- [10] B. Kimy, et al., "Non-orthogonal multiple access in a downlink multiuser beamforming system," in *Proc. IEEE Military Commun. Conf.*, San Diego, CA, Nov. 2013, pp. 1278–1283.
- [11] Y. Liu, et al., "Nonorthogonal multiple access for 5G and beyond," *Proc. IEEE*, vol. 105, no. 12, pp. 2347–2381, Dec. 2017.
- [12] J. Choi, "Non-orthogonal multiple access in downlink coordinated two-point systems," *IEEE Commun. Lett.*, vol. 18, no. 2, pp. 313–316, Feb. 2014.
- [13] Z. Ding, H. Dai, and H. V. Poor, "Relay selection for cooperative NOMA," *IEEE Wireless Commun. Lett.*, vol. 5, no. 4, pp. 416–419, Aug. 2016.
- [14] Z. Yang, Z. Ding, Y. Wu, and P. Fan, "Novel relay selection strategies for cooperative NOMA," *IEEE Trans. Veh. Technol.*, vol. 66, no. 11, pp. 10 114–10 123, 2017.
- [15] P. Xu, Z. Yang, Z. Ding, and Z. Zhang, "Optimal relay selection schemes for cooperative NOMA," *IEEE Trans. Veh. Technol.*, vol. 67, no. 8, pp. 7851–7855, 2018.
- [16] K. J. Kim, M. D. Renzo, H. Liu, P. V. Orlik, and H. V. Poor, "Performance analysis of distributed single carrier systems with distributed cyclic delay diversity," *IEEE Trans. Commun.*, vol. 65, no. 12, pp. 5514–5528, Dec. 2017.
- [17] K. J. Kim, M. D. Renzo, H. Liu, T. A. Tsiftsis, P. V. Orlik, and H. V. Poor, "Distributed cyclic delay diversity systems with spatially distributed interferers," *IEEE Trans. Wireless Commun.*, vol. 18, no. 4, pp. 2066–2079, Jun. 2019.
- [18] K. J. Kim, H. Liu, Z. Ding, P. V. Orlik, and H. V. Poor, "Diversity gain analysis of distributed CDD systems in non-identical fading channels," *IEEE Trans. Commun.*, 2020, under publication.
- [19] K. J. Kim, H. Liu, M. D. Renzo, and H. V. Poor, "Performance analysis of spectrum sharing systems with distributed CDD," in *Proc. 2018 IEEE GLOBECOM*, Abu Dhabi, UAE, Dec. 2018, pp. 1–6.
- [20] K. J. Kim, H. Liu, M. Wen, M. D. Renzo, and H. V. Poor, "Outage probability analysis of spectrum sharing systems with distributed cyclic delay diversity," *IEEE Trans. Commun.*, vol. 67, no. 6, pp. 4435–4449, Jun. 2019.
- [21] K. J. Kim, H. Liu, M. D. Renzo, P. V. Orlik, and H. V. Poor, "Secrecy analysis of distributed CDD-based cooperative systems with deliberate interference," *IEEE Trans. Wireless Commun.*, vol. 12, no. 17, pp. 7865–7878, Dec. 2018.
- [22] K. J. Kim, H. Liu, M. Wen, P. Orlik, and H. V. Poor, "Secrecy performance analysis of distributed asynchronous cyclic delay diversity-based cooperative single carrier systems," *IEEE Trans. Commun.*, vol. 68, no. 5, pp. 2680–2694, May 2020.
- [23] H. Liu, T. A. Tsiftsis, K. J. Kim, K. S. Kwak, and H. V. Poor, "Rate splitting for asynchronous uplink NOMA systems with cyclic prefixed single carrier," in *Proc. IEEE Int. Conf. Commun. Workshops*, Shanghai, China, May 2019, pp. 1–6.
- [24] H. Liu, T. A. Tsiftsis, K. J. Kim, K. S. Kwak, and H. V. Poor, "Rate splitting for uplink NOMA with enhanced fairness and outage performance," *IEEE Trans. Wireless Commun.*, vol. 19, no. 7, pp. 4657–4670, Jul. 2020.
- [25] H. Liu, Z. Ding, K. J. Kim, K. S. Kwak, and H. V. Poor, "Decode-and-forward relaying for cooperative NOMA systems with direct links," *IEEE Trans. Wireless Commun.*, vol. 12, no. 17, pp. 8077–8093, Dec. 2018.

- [26] H. T. Nguyen, T. Q. Duong, and W. J. Hwang, "Multiuser relay networks over unreliable backhaul links under spectrum sharing environment," *IEEE Commun. Lett.*, vol. 21, no. 10, pp. 2314–2317, Oct. 2017.
- [27] S. Lee, J. Kang, S. Jeong, J. Kang, and S. Al-Araji, "Joint design of precoder and backhaul quantizer in cooperative cognitive radio networks," *IEEE Trans. Veh. Technol.*, vol. 66, no. 2, pp. 1871–1875, 2017.
- [28] K. J. Kim, T. Khan, and P. Orlik, "Performance analysis of cooperative systems with unreliable backhauls and selection combining," *IEEE Trans. Veh. Technol.*, vol. 66, no. 3, pp. 2448–2461, Mar. 2017.
- [29] H. Li, J. Hajipour, A. Attar, and V. C. M. Leung, "Efficient HetNet implementation using broadband wireless access with fiber-connected massively distributed antennas architecture," *IEEE Wireless Commun.*, vol. 18, no. 3, pp. 72–78, Jun. 2011.
- [30] X. Li, X. Ge, X. Wang, J. Cheng, and V. C. M. Leung, "Energy efficiency optimization: Joint antenna-subcarrier-power allocation in OFDM-DASs," *IEEE Trans. Wireless Commun.*, vol. 15, no. 11, pp. 7470–7483, Nov. 2016.
- [31] M.-L. Tham, S. F. Chien, D. W. Holtby, and S. Alimov, "Energy-efficient power allocation for distributed antenna systems with proportional fairness," *IEEE Trans. Green Commun. Netw.*, vol. 1, no. 2, pp. 145–157, Jun. 2017.
- [32] R. Heath, S. Peters, Y. Wang, and J. Zhang, "A current perspective on distributed antenna systems for the downlink of cellular systems," *IEEE Commun. Mag.*, pp. 161–167, Apr. 2013.
- [33] X. Tao, X. Xu, and Q. Cui, "An overview of cooperative communications," *IEEE Commun. Mag.*, pp. 65–71, Jun. 2012.
- [34] Y. Zeng and T. S. Ng, "Pilot cyclic prefixed single carrier communication: channel estimation and equalization," *IEEE Signal Process. Lett.*, vol. 12, no. 1, pp. 56–59, Jan. 2005.
- [35] F. Gao, A. Nallanathan, and C. Tellambura, "Blind channel estimation for cyclic-prefixed single-carrier systems by exploiting real symbol characteristics," *IEEE Trans. Veh. Technol.*, vol. 56, no. 5, pp. 2487–2498, Sep. 2007.
- [36] K. J. Kim and T. A. Tsiftsis, "Performance analysis of QRD-based cyclically prefixed single-carrier transmissions with opportunistic scheduling," *IEEE Trans. Veh. Technol.*, vol. 60, no. 1, pp. 328–333, Jan. 2011.
- [37] K. J. Kim, Y. Yue, R. A. Iltis, and J. D. Gibson, "A QRD-M/Kalman Filter-based detection and channel estimation algorithm for MIMO-OFDM systems," *IEEE Trans. Wireless Commun.*, vol. 4, pp. 710–721, Mar. 2005.
- [38] IEEE P802.11ad/D0.1, "Wireless LAN medium access control (MAC) and physical layer (PHY) specifications: Enhancements for very high throughput in the 60GHz band," Jun. 2010.
- [39] S. Kato, H. Harada, R. Funada, T. Baykas, C. S. Sum, J. Wang, and M. A. Rahman, "Single carrier transmission for multi-gigabit 60-GHz WPAN systems," *IEEE J. Sel. Areas Commun.*, vol. 27, no. 8, pp. 1466–1478, Oct. 2009.
- [40] C. Studer, M. Wenk, and A. Burg, "MIMO transmission with residual transmit-RF impairments," in *Proc. ITG Work. Smart Ant.*, 2010, pp. 189–196.
- [41] M.-S. Alouini and M. K. Simon, "An MGF-based performance analysis of generalized selection combining over Rayleigh fading channels," *IEEE Trans. Commun.*, vol. 48, no. 3, pp. 401–415, Mar. 2000.
- [42] Y. Ma and C. C. Chai, "Unified error probability analysis for generalized selection combining in Nakagami fading channels," *IEEE J. Sel. Areas Commun.*, vol. 18, no. 11, pp. 2198–2210, Nov. 2000.
- [43] Wolfram Research Inc. The Mathematical Functions Site. Accessed: Oct.13, 2019. [Online]. Available: <http://functions.wolfram.com>
- [44] A. P. Prudnikov, Y. A. Brychkov, and O. I. Marichev, *Integral and Series. Vol. 3: More Special Functions*, 3rd ed. London: Gordon and Breach, 1992.
- [45] I. Shafique, S. Al-Ahmadi, F. Yilmaz, M.-S. Alouini, and H. Yanikomeroglu, "A new formula for the BER of binary modulations with dual-branch selection over generalized- K composite fading channels," *IEEE Trans. Commun.*, vol. 59, no. 10, pp. 2654–2658, Oct. 2011.
- [46] 3GPP, TR 36.828 (V11.0.0), "Further enhancements to lte time division duplex (TDD) for downlink-uplink (DL-UL) interference management and traffic adaptation," Jun. 2012.
- [47] D. Tse and P. Viswanath, *Fundamental of Wireless Communications*. Cambridge, UK: Cambridge University Press, 2005.
- [48] I. S. Gradshteyn and I. M. Ryzhik, *Table of Integrals, Series, and Products*. New York: Academic Press, 2007.
- [49] H. Chergui, M. Benjillali, and S. Saoudi, "Performance analysis of project-and-forward relaying in mixed MIMO-pinchole and Rayleigh dual-hop channel," *IEEE Commun. Lett.*, vol. 20, no. 3, pp. 610–613, Mar. 2016.